

Quarl: A Learning-Based Quantum Circuit Optimizer

ZIKUN LI, Carnegie Mellon University, USA

JINJUN PENG, Tsinghua University, China

YIXUAN MEI, Tsinghua University, China

SINA LIN, Microsoft, USA

YI WU, Tsinghua University, China

ODED PADON, VMware Research, USA

ZHIHAO JIA, Carnegie Mellon University, USA

Optimizing quantum circuits is challenging due to the very large search space of functionally equivalent circuits and the necessity of applying transformations that temporarily decrease performance to achieve a final performance improvement. This paper presents Quarl, a learning-based quantum circuit optimizer. Applying reinforcement learning (RL) to quantum circuit optimization raises two main challenges: the large and varying action space and the non-uniform state representation. Quarl addresses these issues with a novel neural architecture and RL-training procedure. Our neural architecture decomposes the action space into two parts and leverages graph neural networks in its state representation, both of which are guided by the intuition that optimization decisions can be mostly guided by local reasoning while allowing global circuit-wide reasoning. Our evaluation shows that Quarl significantly outperforms existing circuit optimizers on almost all benchmark circuits. Surprisingly, Quarl can learn to perform rotation merging—a complex, non-local circuit optimization implemented as a separate pass in existing optimizers.

1 INTRODUCTION

Quantum computing presents a novel paradigm that enables significant acceleration over classical counterparts in a wide range of applications, such as quantum simulation (Cao et al., 2019), integer factorization (Monz et al., 2016), and machine learning (Biamonte et al., 2017). However, programming quantum computers is a challenging task due to the scarcity of qubits and the diverse forms of noise that affect the performance of near-term intermediate-scale quantum (NISQ) devices.

Quantum programs are commonly represented as *quantum circuits*, such as the one shown in Figure 1, where each horizontal wire represents a qubit and boxes on these wires represent quantum gates. To enhance the success rate of executing a circuit, a common form of optimization is applying *circuit transformations*, which replace a subcircuit matching a specific pattern with a functionally equivalent subcircuit that has better performance (e.g. fidelity, depth).

Prior research has proposed two approaches for performing circuit transformations on an input circuit. The first approach is the use of *rule-based* strategies, which are employed by many quantum compilers such as Qiskit (Aleksandrowicz et al., 2019), t|ket (Sivarajah et al., 2020), and Quilc (Skilbeck et al., 2020). These strategies involve the greedy application of a set of circuit transformations that are manually designed by quantum computing experts to improve the performance of quantum circuits. The second approach, as introduced in recent work (Pointing et al., 2021, Xu et al., 2022a,c), is a *search-based* approach that explores a search space of circuits that are functionally equivalent to the input circuit. Quartz (Xu et al., 2022c) automatically generates and verifies circuit transformations for a given gate set, which preserves equivalence but may not necessarily improve performance. To optimize an input circuit, Quartz employs a cost-based backtracking search algorithm to apply these transformations and discover an optimized circuit.

Authors' addresses: Zikun Li, Carnegie Mellon University, Pittsburgh, PA, USA, zikunl@andrew.cmu.edu; Jinjun Peng, Tsinghua University, Beijing, China, mail@co1in.me; Yixuan Mei, Tsinghua University, Beijing, China, meiyixuan2000@gmail.com; Sina Lin, Microsoft, Mountain View, CA, USA, silin@microsoft.com; Yi Wu, Tsinghua University, Beijing, China, jxwuyi@gmail.com; Oded Padon, VMware Research, Palo Alto, CA, USA, oded.padon@gmail.com; Zhihao Jia, Carnegie Mellon University, Pittsburgh, PA, USA, zhihao@cmu.edu.

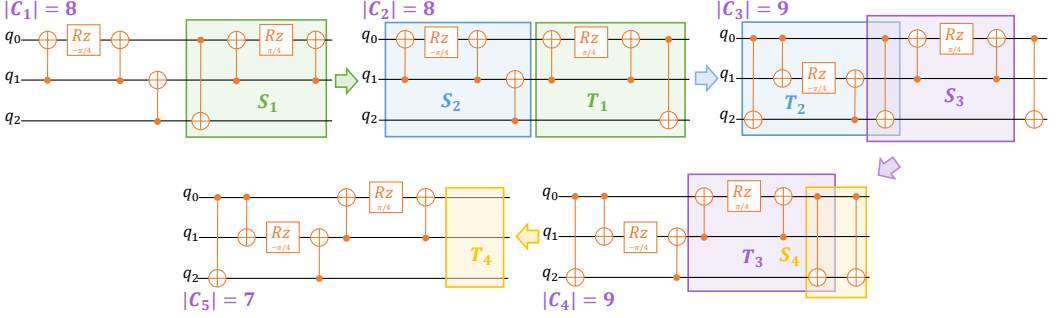


Fig. 1. A quantum circuit optimization with four transformations, one of which increases the cost as an intermediate step. Each arrow indicates a transformation, whose source and target sub-circuits are highlighted by boxes in the same color.

Although existing approaches improve the performance of quantum circuits, they are limited by the following challenges in transformation-based quantum circuit optimization.

Planar optimization landscape. The set of circuits that can be reached from an input circuit by iteratively applying verified, equivalence-preserving transformations comprises the search space in quantum circuit optimization. However, finding the optimal circuit in this space is challenging due to the space’s size, which makes exhaustive exploration infeasible, and the inability of the cost function (derived from a selected performance metric) to provide enough guidance for a greedy approach. This scenario is referred to as a *planar optimization landscape* since the path from one circuit to another with lower cost often contains many steps in which the cost remains unchanged. (Plateaus of this sort are also present in classic program optimization (Koenig et al., 2021).)

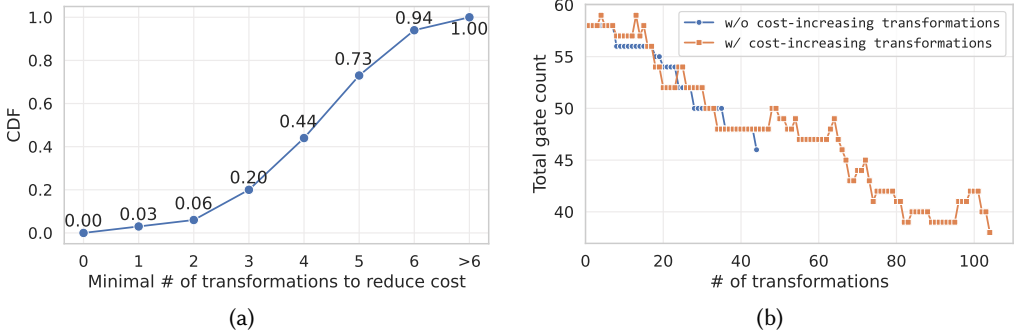


Fig. 2. An analysis on the search space of barenc0_tof_3. (a) CDF of the minimal number of transformations needed to reduce gate count. (b) The optimization trace of the best discovered circuits when including and excluding cost-increasing transformations.

To illustrate the challenge of discovering an optimal circuit in the search space, we analyze the search space of a relatively small circuit barenc0_tof_3 (Nam et al., 2018). The circuit includes three Toffoli gates, implemented with 58 gates in the Nam gate set ($CNOT$, X , H , Rz). We consider the 6,206 transformations discovered by Quartz (Xu et al., 2022c) for the Nam gate set and exhaustively find all circuits reachable within seven transformation applications. Of these roughly 162000000 circuits, we randomly sample 200 circuits and analyze the optimization landscape around them.

Specifically, for each sampled circuit C , we perform a breadth-first search (BFS) to determine the shortest path from C to a circuit C' with a lower cost (using the total number of gates as the cost function). That is, we determine the radius of the planar optimization landscape around C . The BFS is performed up to a radius of 6, so we either find the exact radius or conclude that it is greater than 6. Notably, it is guaranteed that all of the 200 circuits can be optimized because their cost is larger than the optimal cost. The results are summarized in Figure 2. For more than half of the sampled circuits, reducing the total gate count requires applying more than 4 transformations, and 6% of the sampled circuits require more than 6 transformations to improve performance. While we could exhaustively explore transformation sequences of length seven for `barenco_tof_3`, this would not be practical for larger circuits with hundreds of gates or more. Therefore, in the absence of guidance from the cost function, it is natural to consider a learning-based approach to learn a good heuristic that can guide the application of transformations towards a lower-cost circuit.

Cost-increasing transformations. One of the challenges in optimizing quantum circuits is the need to use transformations that may temporarily increase the cost. For example, the second transformation in Figure 1 increases the gate count from 8 to 9, which is necessary to enable the subsequent transformations that ultimately reduce the gate count to 7. Cost-increasing transformations are crucial to discovering highly optimized circuits. To illustrate this point, we compare the performance of the best discovered circuits with and without cost-increasing transformations in Figure 2b. Without using cost-increasing transformations for circuit `barenco_tof_3`, the best circuit that can be discovered in our experiments has 46 gates, while involving cost-increasing transformations can further reduce the gate count to 36. However, determining when and where to apply cost-increasing transformations is non-trivial, as these transformations are only beneficial when combined with other transformations that eventually reduce the cost.

Our approach. This paper presents Quarl, a learning-based quantum circuit optimizer. Specifically, Quarl utilizes reinforcement learning (RL) to guide the application of quantum circuit transformations. In the RL task, each circuit is defined as a state, and each application of a transformation is considered an action. By adopting this formulation, Quarl can learn to identify circuit optimization opportunities and perform long sequences of transformations to achieve them.

The first challenge we must address in applying RL to circuit optimization is the large action space. For example, when learning to apply the 6,206 transformations discovered by Quartz (Xu et al., 2022c) on a thousand-gate circuit, there may be millions of possible actions (i.e., ways to match a transformation to a subcircuit of the current circuit). Such a large action space would degrade the training efficiency of most RL algorithms. To deal with this issue, we propose a *hierarchical action space* that uses a gate-transformation pair to uniquely identify a potential transformation application, so that the RL agent first chooses a gate and then a transformation to apply. This decomposition allows Quarl to use two much smaller sub-action spaces, enabling effective training. To effectively train the RL agent to select both a gate and a transformation, we propose *hierarchical advantage estimation* (HAE), which allows Quarl to train two policies with a single *actor-critic* architecture. Quarl combines HAE with *proximal policy optimization* (PPO) (Schulman et al., 2017) to jointly train the gate- and transformation-selecting policies.

The second challenge for RL-based quantum circuit optimization is state representation. An RL application typically represents states as vectors in a fixed, high-dimensional space. Unlike most RL tasks whose states have relatively uniform structure, a state in our setting is a quantum circuit whose size and topology depend on the input circuit and change at each step during the optimization process, making it non-trivial to design a fixed, uniform state representation. A key insight behind Quarl’s approach is to leverage the *locality* of quantum circuit transformations, that is, the decision of applying a transformation at a certain location is largely guided by the local

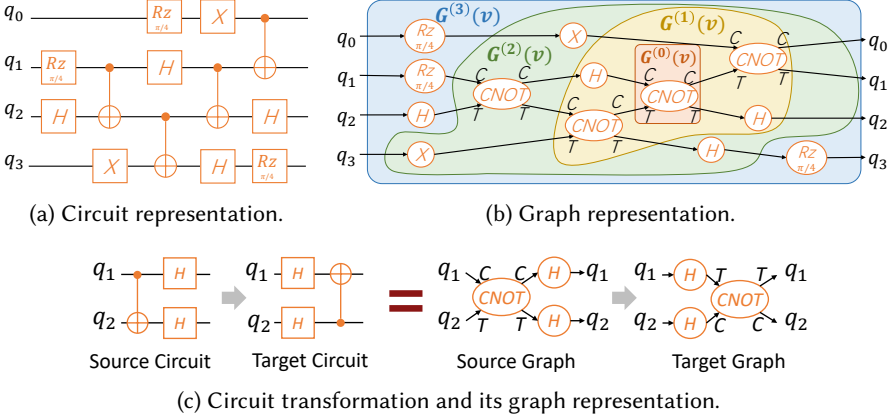


Fig. 3. A quantum circuit (a) and its graph representation (b). For each CNOT, C and T correspond to the control and target qubits. $G^{(k)}(v)$ shows the k -hop neighborhood (see Section 4.1) for the CNOT gate identified by $G^{(0)}(v)$. (c) illustrates a circuit transformation and its graph representation.

environment at that location. Based on this insight, Quarl uses a *graph neural network* (GNN)-based approach to represent the local environment of each gate. Although each representation encodes the local environment of only one gate, combining all gate representations allows Quarl to identify optimization opportunities across the entire circuit. A key advantage of our learned gate-level representations is that they are independent to the circuit size and generalize well to unseen circuits. By combining this local decision making with global circuit-wide fine-tuning, we aim to achieve a balance of both local and global guidance for the optimization process.

The evaluation results demonstrate the superior performance of Quarl over existing circuit optimizers for almost all circuits. For example, on the Nam gate set, Quarl achieves an average reduction of 35.8% and 33.9% in total gate count and CNOT gate count, respectively (geometric mean), while the best existing optimizers achieve reductions of only 28.3% and 20.6%. On the IBM gate set, Quarl achieves an average reduction of 36.6% and 21.3% in total gate count and CNOT gate count, respectively (geometric mean), while the best existing optimizers achieve reductions of 20.1% and 7.7%. Furthermore, Quarl improves circuit fidelity by up to 4.66 \times (with an average fidelity improvement of 1.37 \times) on the IBM gate set, while the best existing optimizer only improves circuit fidelity by 1.07 \times . Notably, the evaluation also reveals that Quarl can automatically discover rotation merging, a non-local circuit optimization, from its own exploration, while existing optimizers require manual implementation of this technique.

The remainder of this paper is organized as follows. Section 2 provides background information on transformation-based quantum circuit optimization and reinforcement learning. Section 3 outlines the key challenges associated with applying reinforcement learning to quantum circuit optimization and describe our approach for addressing them. The main technical contributions of this paper are presented in Section 4 that presents Quarl’s neural architecture, and Section 5 that presents Quarl’s training methodology. Empirical evaluations are presented in Section 6, and related work are discussed Section 7.

2 BACKGROUND

Graph representation of quantum circuits. We adopt the graph representation of quantum circuits from prior work (Xu et al., 2022c). As illustrated in Figures 3a and 3b, a circuit C is represented as a directed acyclic labeled graph $G = (V, E)$. Each gate with q qubits is represented as a node $v \in V$

with q in- and out-edges, and each edge $e \in E$ represents a connection of two adjacent gates on a qubit. Nodes are labeled with gate types, and edges are labeled to distinguish different qubits of a multi-qubit gate (e.g., the control and target qubits of a CNOT gate).

Transformation-based circuit optimization. To improve the performance of quantum circuits, a common form of optimization is *circuit transformations*, which replace a subcircuit matching a specific pattern with a distinct equivalent subcircuit. In the graph representation, a subcircuit correspond to a convex subgraph (Xu et al., 2022c, p.8); a transformation is represented as a pair of connected graphs (G, G') representing equivalent circuits as illustrated in Figure 3c, and applying it to a circuit C amounts to finding a convex subgraph of C that is isomorphic to G , and then replacing it by G' to yield a new circuit C' . An application of a transformation (G, G') to a circuit C is uniquely determined once a single gate $g \in G$ is matched with a gate $g_C \in C$, due to the unique edge labeling and the fact that G is always a connected graph.

Reinforcement learning (RL). RL is a class of machine learning algorithms that train an agent to take actions in an environment while optimizing a given objective. An RL problem is formalized as a Markov decision process defined by a tuple (S, A_s, P, r, γ) , where S is the state space of the environment, A_s is the action space for the agent at state $s \in S$, $P(s'|s, a)$ defines the probability of the state transiting from s to s' if the agent takes the action a , $r(s', s, a)$ defines the immediate reward of the transition from state s to state s' by action a , and $\gamma \in (0, 1)$ is the discounted factor used to give more immediate rewards greater weight than future rewards. Each state-action pair is a *step*, and a sequence of steps is a *trajectory*, denoted as $\tau = (s_0, a_0, s_1, a_1, \dots)$. The *return* of a trajectory $\tau = (s_0, a_0, s_1, a_1, \dots)$ is the discounted cumulative reward along the trajectory, given by $R_\tau = \sum_{t=0} \gamma^t r_t$, where $r_t = r(s_{t+1}, s_t, a_t)$ denotes the reward at step t . We sometimes use R_t for the discounted cumulative reward starting from step t in the trajectory, which is $R_t = \sum_{t'=t} \gamma^{t'-t} r_{t'}$.

RL agents aim to learn a *policy* to maximize the return through trial and error, by first collecting trajectories and then optimizing the policy based on the actions taken and the returns observed. Formally, a *policy* is a function π that maps each state to a probability distribution over valid actions. A policy induces a probability distribution over trajectories starting at a given state (i.e., trajectories *generated* by the policy), where a_t is sampled according to $\pi(s_t)$ and s_{t+1} is sampled according to $P(s_{t+1}|s_t, a_t)$. A policy parameterized by θ is denoted as $\pi(\cdot|s; \theta)$ or π_θ . The learning objective in RL is to maximize the expected return of trajectories generated by the policy π_θ , i.e., $J(\theta) = E_{\tau \sim \pi_\theta} [R_\tau]$.

Policy gradient methods (Sutton et al., 1999) optimize this objective by gradient ascent over $J(\theta)$ w.r.t. θ . By the policy gradient theorem (Sutton et al., 1999), an equivalent formulation in the form of a loss function can be expressed as $L^{PG}(\theta) = E_{\tau \sim \pi_\theta} [\sum_t \log \pi(a_t|s_t; \theta) A(s_t, a_t)]$, whose gradient is equivalent to $\nabla J(\theta)$ and can be estimated by sampling τ . $A(s_t, a_t)$ in $L^{PG}(\theta)$ is the *advantage*, defined as $A(s, a) = Q^\pi(s, a) - V^\pi(s)$, where $Q^\pi(s, a) = E[R_\tau | s_0 = s, a_0 = a]$ is the Q-function (i.e., the expected return starting from state s and taking action a), and $V^\pi(s) = E[R_\tau | s_0 = s]$ is the expected return starting from state s . Advantage measures how much better the agent can get by taking a specific action at a state than average. By gradient ascent, actions are *reinforced* based on their advantages (i.e. the probability of an action increases if its advantage is positive, and drops otherwise). The empirical advantage \hat{A}_t is often estimated as $\hat{A}(s_t, a_t) = R_t - V^\pi(s_t)$ over a sampled trajectory, where R_t is the return, which is a sampled estimation of $Q^\pi(s_t, a_t)$, and $V^\pi(s_t)$ is typically approximated by training another neural network. Such a framework is also referred to as the *actor-critic* method, where actor denotes the policy and critic denotes the value network (Mnih et al., 2016).

Proximal policy optimization (PPO). PPO is a popular variant of policy gradient methods that achieve state-of-the-art performances in a wide range of applications (Schulman et al., 2017). PPO

propose an clipped surrogate objective:

$$L^{CLIP}(\theta) = E_{\tau \sim \pi_{\theta_{old}}} \left[\sum_t \min(\rho_{\theta}(s_t, a_t) \hat{A}_t, \text{clip}(\rho_{\theta}(s_t, a_t), \epsilon) \hat{A}_t) \right] \quad (1)$$

where $\rho_{\theta}(s, a) = \frac{\pi_{\theta}(a|s)}{\pi_{\theta_{old}}(a|s)}$, \hat{A}_t denotes the estimated advantage $\hat{A}(s_t, a_t)$ at step t over trajectory τ generated by $\pi_{\theta_{old}}$, and $\text{clip}(\rho, \epsilon) = \min(1 + \epsilon, \max(1 - \epsilon, \rho))$ is the clip function used by PPO (Schulman et al., 2017, Eq. 7).

3 CHALLENGES AND HIGH-LEVEL APPROACH

Applying reinforcement learning to optimize quantum circuits presents several challenges unique to this problem setting. This section presents these challenges and the key ideas Quarl uses to overcome them. In the sequel, we assume a fixed gate set, set of equivalence-preserving transformations, and cost function. We formulate quantum circuit optimization as a Markov decision process (S, A_s, P, r, γ) as follows. S is the set of circuits over the given gate set. For a circuit $C \in S$, A_C includes all valid applications of transformations on C . Applying a transformation (i.e., an action) a to a circuit C deterministically defines a new circuit C' ; therefore we let $P(C'|C, a) = 1$ and $P(C''|C, a) = 0$ for $C'' \neq C'$. Finally, the reward function is given by the cost difference between the circuits before and after a transformation: $r(C, a) = \text{COST}(C) - \text{COST}(C')$.

3.1 Challenge 1: Action Space

Directly applying existing policy gradient methods to our setting requires the RL agent to learn a policy that can simultaneously select a transformation and a subcircuit to apply the transformation for a given circuit. However, learning such a policy is challenging due to the very large action space. For example, when learning to apply the 8,664 transformations discovered by Quartz (Xu et al., 2022c) on a thousand-gate circuit, there can be up to millions of actions (i.e., possible applications of the transformations) for a given state (i.e., circuit). The large action space degrades the training efficiency of the RL agent, since a training sample only directly updates the probability of a single action, and exploring a large action space requires a huge amount of training samples. Moreover, the action space of a state depends on its graph structure, which changes at each step.

Solution. For a circuit C , Quarl decomposes its action space A_C into two ‘‘subspaces’’: a position space P_C and a transformation space X . P_C includes all gates in C , and X contains all transformations. (Recall that a subcircuit matching a transformation can be determined by matching a single gate, see Section 2.) Under this decomposition, A_C is a subset of $P_C \times X$, and we can train separate policies for P_C and X .

3.2 Challenge 2: State Representation

At the core of most RL algorithms is a representation of states as high-dimensional vectors. However, unlike most RL tasks whose states have a uniform structure, a state in our setting is a quantum circuit whose size and topology depend on the input circuit and may change at each step during the optimization process. Therefore, designing a uniform state representation for quantum circuits is challenging. A straightforward approach would be to directly represent each quantum circuit as a high-dimensional vector. However, due to the diversity of quantum circuits, this approach leads to learned representations that are highly tailored to the circuits used in training and do not generalize well to unseen circuits.

Solution. A key insight for addressing this challenge is leveraging the *locality* of circuit transformations, that is, while the overall optimization strategy depends on the entire circuit, we

hypothesize that the decision of applying a transformation at a gate can be largely guided by the local environment of the gate. Based on this hypothesis, we design a neural architecture that relies on local decision making when selecting a gate to apply a transformation. In particular, Quarl uses a K -layer graph neural network (GNN) to represent the K -hop neighborhood of each gate (see Definition 1). While each representation only encodes a local subcircuit, combining all gates’ representations allows Quarl to collectively represent an entire circuit. A key advantage of our approach is that the representations generated by the GNN is independent of the circuit size and thus can generalize to circuits at different time steps in the optimization process. While our approach localizes the decision making, it still allows global circuit-wide guidance, since we fine-tune the RL agent (including the weights of the GNN) when optimizing a circuit (see Section 5). With this design, we aim to achieve a good balance between local and global decision making in the optimization process.

3.3 Quarl’s Approach

Combining our solutions to the two challenges discussed above, we propose a hierarchical approach to optimizing quantum circuits using RL. Quarl’s neural architecture is outlined in Figure 4. The first stage in processing the current circuit C_t is the *gate representation generator*, which is a graph neural network (GNN) that computes a learned vector representation for the K -hop neighborhood of each gate in C_t (see Section 4.1). Next, based on these learned representations, Quarl’s *gate selector* chooses a gate g_t using a learned *gate-selecting policy*, denoted $\pi_g(\cdot|C_t; \theta_g)$, which is a probability distribution over all gates in C_t (see Section 4.2). Finally, the learned representation of g_t is fed into Quarl’s *transformation selector*, which selects a transformation using a learned *transformation-selecting policy*, denoted $\pi_x(\cdot|C_t, g_t; \theta_x)$, which is a probability distribution over all valid transformations at g_t (see Section 4.3).

The gate- and transformation-selecting policies are trained jointly in Quarl with a combined actor-critic architecture. Specifically, the actor network learns the transformation-selecting policy, and the critic network acts both as a value estimator for the transformation-selecting policy and as a predictor for the gate-selecting policy. In other words, the transformation-selecting policy is the *only* policy whose parameters are updated by gradient ascent and whose actions (i.e., transformation selections) are reinforced. The critic network learns to estimate the value of the state derived by applying the transformation-selecting policy, which is the K -hop neighborhood of a gate. The gate-selecting policy evaluates all gates with the value estimator of the transformation-selecting policy and selects (with high probability) a high-value gate. Intuitively, the value estimator is suitable to form the gate-selecting policy, because high value indicates high optimization opportunity.

Compared to a straightforward PPO approach, where the actor learns both π_g and π_x , and the critic learns to estimate the value of an entire circuit, our method has fix-sized state (the K -hop neighborhood) for both the actor and critic, and a fixed and relatively small action space for the transformation-selecting policy. These advantages ultimately make our policies easier to train. However, our specialized architecture requires a different advantage estimator from standard PPO, which we develop in Section 5.

4 QUARL’S NEURAL ARCHITECTURE

We introduce Quarl’s gate representation generator in Section 4.1, the gate selector in Section 4.2, and the transformation selector in Section 4.3.

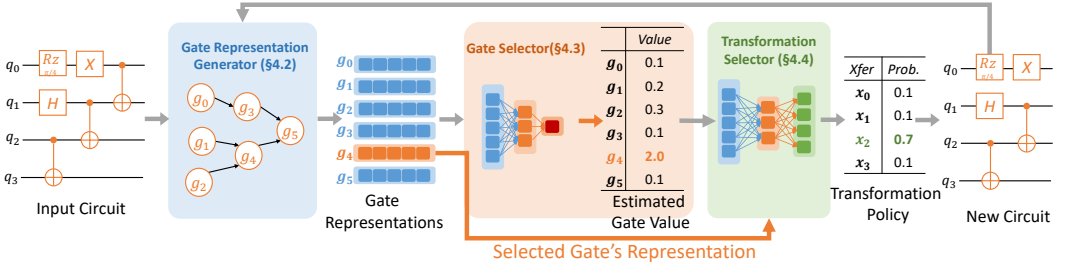


Fig. 4. The neural architecture of Quarl’s RL agent. The arrows indicate the control flow.

4.1 Gate Representation Generator

For an input circuit C , Quarl uses a graph neural network (GNN) with K layers to learn to represent the K -hop neighborhood of each gate in C as a high-dimensional vector. Our GNN architecture follows GraphSAGE (Hamilton et al., 2017).

DEFINITION 1 (k -HOP NEIGHBORHOOD). For a node v in graph G , its k -hop neighborhood, denoted $G^{(k)}(v)$, is the subgraph of G that includes all nodes within k (undirected) hops from v .

Figure 3b shows the k -hop neighborhood for a selected gate (identified by $G^{(0)}(v)$) and different values of $k \in \{1, 2, 3\}$.

The GNN architecture takes as inputs (1) a circuit represented as a graph, (2) gate-level features (i.e., the type of each gate), and (3) edge-level features (i.e., the direction of each edge and the qubits it connects to). Let $h_g^{(k)}$, $k \in \{1, \dots, K\}$ denote the representation of the k -hop neighborhood of gate g outputted by the k th GNN layer, let $h_g^{(0)}$ denote the input features of the first GNN layer for g (i.e., an embedding of g ’s gate type), and let e_{uv} denote the edge features of the edge between node u and v . $h_g^{(k)}$ is computed by taking $h_u^{(k-1)}$ and e_{ug} as inputs, where u is a neighbor gate of g . Each GNN layer includes an *aggregation* phase, which first gathers the representations of each gate’s neighbors from the previous GNN layer, and an *update* phase, which computes a new representation for each gate by combining its previous representation and the aggregated neighborhood representations.

Aggregation phase. Let $N(g)$ denote gate g ’s neighbors in the graph (i.e. a set of gates that share an in- or out-edge with g). For each gate g , the aggregation phase at layer k takes as inputs $h_u^{(k-1)}$ and e_{ug} ($u \in N(g)$) and computes an aggregated representation of g ’s neighbors $a_g^{(k)}$ with a multi-layer perceptron (MLP) (Gardner and Dorling, 1998). The neural architecture of the aggregate phase is formalized as follows:

$$a_g^{(k)} = \sum_{u \in N(g)} \sigma(W_a^{(k)} \cdot \text{concat}(h_u^{(k-1)}, e_{ug}) + b_a^{(k)}) \quad (2)$$

where $W_a^{(k)}$ and $b_a^{(k)}$ denote the weights of the MLP in the aggregation phase of the k -th layer, and $\sigma(\cdot)$ is the ReLU function (Agarap, 2018).

Update phase. For each gate g , the update phase computes a new representation $h_g^{(k)}$ by combining g ’s representation from the previous GNN layer (i.e., $h_g^{(k-1)}$) and the aggregated neighbor representation (i.e., $a_g^{(k)}$). The neural architecture of the update phase is formalized as follows:

$$h_g^{(k)} = \sigma(W_u^{(k)} \cdot \text{concat}(h_g^{(k-1)}, a_g^{(k)})) \quad (3)$$

where $W_u^{(k)}$ denotes the weight matrix of the MLP in the update phase.

Note that using more GNN layers allows Quarl to represent a larger neighborhood of each gate but introduces more trainable parameters, which requires more time and resource to train (see Section 5). Section 6 analyzes the choice of K .

4.2 Gate Selector

The gate selector is composed of two parts: a *gate value predictor* and a *gate sampler*. The gate value predictor predicts the on-policy value $V^{\pi_x}(C, g)$ (see Section 5.3) of gate g on circuit C for the transformation selecting policy π_x . The gate value predictor takes as an input $h_g^{(K)}$, which represents the K -hop neighborhood of g on circuit C , and outputs $V^{\pi_x}(C, g; \theta_g)$, which approximates $V^{\pi_x}(C, g)$, and θ_g denotes the trainable parameters of the predictor. The predictor uses a multi-layer perceptron (MLP) (Hinton, 1987) in our current implementation.

Our gate selecting policy π_g is formed by applying a temperature softmax (He et al., 2018) to the outputs of the gate value predictor, which is parameterized as follows:

$$\pi_g(g|C; \theta_g) = \frac{\exp(V^{\pi_x}(C, g; \theta_g)/t)}{\sum_{g' \in C} \exp(V^{\pi_x}(C, g'; \theta_g)/t)} \quad (4)$$

where $\pi_g(g|C; \theta_g)$ denotes the probability of choosing g in circuit C , and t is a temperature parameter for the softmax function. The temperature $t \in (0, +\infty)$ balances exploration and exploitation. Specifically, when t is larger, π_g selects gates with increased randomness and becomes more explorative. On the other hand, when t becomes smaller, π_g becomes more exploitative and tends to select the gate with the highest estimated value. Balancing exploration and exploitation across different circuits requires circuit-specific temperatures. For a specific circuit C , we set the temperature t as

$$t = 1/\ln \frac{\lambda(|C| - 1)}{1 - \lambda}, \lambda \in (0, 1) \quad (5)$$

where $|C|$ is the number of gates in circuit C and λ is a measure of exploitation. Specifically, we set t such that even if there is only one gate with a value close to 1 (representing an optimization opportunity to reduce cost by 1), and the values of all other gates are close to 0 (representing no optimization opportunity), the gate selector samples the high-value gate with probability $\sim \lambda$.

4.3 Transformation Selector

Given a circuit C and a gate g , Quarl’s *transformation selector* chooses a transformation to apply at g . The transformation selector is an MLP, which takes as an input the representation of the selected gate $h_g^{(K)}$, and outputs a probability distribution $\pi_x(\cdot|C, g; \theta_x)$ over the entire set of transformations X , where θ_x denotes the trainable parameters of the transformation selector. The final output of the MLP is followed by a masked softmax layer. The mask is generated by the circuit transformation engine by checking every transformation in X to figure out which of them can be applied to gate g . The masked softmax function filters out invalid transformations.

5 TRAINING AND INFERENCE METHODOLOGY

To train Quarl’s neural architecture with PPO, Section 5.1 introduces *hierarchical advantage estimator*, a novel approach to estimating the actions’ advantages in our problem setting. Algorithm 1 lists Quarl’s RL-based optimization algorithm, which optimizes a circuit by training the RL agent. A training iteration of Quarl consists of two phases: *data collection*, which uses the current RL agent to generate trajectories for RL training (line 5-19), and *agent update*, which uses gradient descent to update the agent’s trainable parameters (line 20-21). The two phases are introduced in

Algorithm 1 Quarl’s RL-based circuit optimization algorithm. B and T are hyper-parameters that specify the number of trajectories to collect in each training iteration and the maximum number of transformations in each trajectory. NOP is a special transformation that stops the current trajectory when selected. Quarl uses α to control data collection (see Section 5.2).

```

1: Inputs: A circuit  $C_{input}$ 
2: Output: An optimized circuit
3:  $C = \{C_{input}\}$  ▷  $C$  is the initial circuit buffer
4: for iteration = 1, ... do
5: ▷ Training data collection
6:    $\mathcal{R} = \emptyset$  ▷ Clear the rollout buffer in each iteration
7:   for  $j = 1, \dots, B$  do
8:     Sample an initial circuit  $C_0^{(j)}$  from  $C$  (see Section 5.2)
9:     for  $t = 1, \dots, T$  do
10:      Compute gate representations  $h_g^{(K)}$  for  $g \in C_{t-1}^{(j)}$ 
11:      Selects gate  $g_t^{(j)}$  using  $\pi_g(\cdot | C_{t-1}^{(j)}; \theta_g)$ 
12:      Selects transformation  $x_t^{(j)}$  using  $\pi_x(\cdot | C_{t-1}^{(j)}, g_t^{(j)}; \theta_x)$ 
13:      Generate new circuit  $C_t^{(j)}$  by applying  $x_t^{(j)}$  at  $g_t^{(j)}$ 
14:      Compute reward  $r_t^{(j)} = \text{COST}(C_{t-1}^{(j)}) - \text{COST}(C_t^{(j)})$ 
15:       $\mathcal{R} = \mathcal{R} \cup \{(C_{t-1}^{(j)}, C_t^{(j)}, g_t^{(j)}, x_t^{(j)}, r_t^{(j)}, V^{\pi_x}(C_{t-1}^{(j)}, g_t^{(j)}; \theta_g), \pi_x(x_t^{(j)} | C_{t-1}^{(j)}, g_t^{(j)}; \theta_x))\}$ 
16:      if  $\text{COST}(C_t^{(j)}) \leq \text{COST}(C_0^{(j)})$  then
17:         $C = C \cup \{C_t^{(j)}\}$ 
18:      if  $x_t^{(j)} = \text{NOP} \vee \text{COST}(C_t^{(j)}) > \alpha \cdot \text{COST}(C_{input})$  then
19:        break ▷ End the trajectory
20:      ▷ Agent update
21:   Update  $\theta_g, \theta_x$  using SGD (loss given by eq. (9)) for  $M$  epochs
22: return  $\text{argmin}_{C \in \mathcal{C}} \text{COST}(C)$ 

```

Sections 5.2 and 5.3, respectively. Finally, Section 5.4 discusses Quarl’s combination of pre-training and fine-tuning to optimize an input circuit.

5.1 Hierarchical Advantage Estimator

As described in Sections 3.3 and 4, Quarl uses a combined actor-critic architecture to jointly train two policies: the gate-selecting policy π_g , which is directly approximated using the values $V^{\pi_x}(C, g)$; and the transformation-selecting policy π_x , on which we apply RL training with an adaptation of PPO. For the transformation-selecting policy π_x , its input is the embedding of the K -hop neighborhood of a gate g on circuit C (i.e., $C^{(K)}(g)$), and its output action is an applicable transformation x at gate g . To update π_x using policy gradient, a key challenge is to estimate the advantage of applying transformation x . In the canonical framework of PPO, the advantage \hat{A}_t of applying x at step t over a sampled trajectory τ is estimated by the difference between the return R_t and the value function, namely $\hat{A}_t = R_t - V^{\pi_x}(C, g)$. However, such a straightforward approach can be problematic in our setting. The value function $V^{\pi_x}(C, g)$ is computed using the GNN embedding over the K -hop neighborhood of gate g , so it represents the *local* value for the neighborhood of g rather than the *global* value of the entire circuit C . Note that when generating a trajectory τ during RL training, our hierarchical policy may choose an arbitrary gate g according to π_g to apply a transformation, so the following steps in τ after x is applied to g can involve gates that are arbitrarily far away

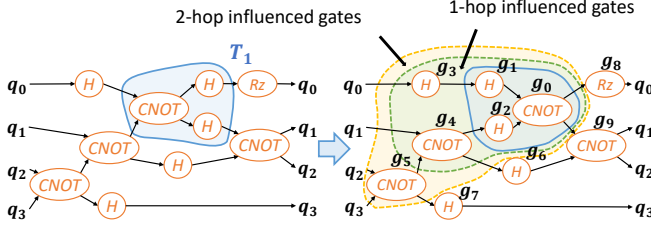


Fig. 5. The ℓ -hop influenced gates of applying the graph transformation in Figure 3c.

from g . Accordingly, the trajectory return R_t is in fact estimating the *global* return over the circuit C rather than the *local* return over the K -hop neighborhood. Therefore, the *multi-step* trajectory return R_t may not be the most appropriate choice for advantage estimation.

In order to obtain an accurate *local* advantage, we propose a *hierarchical advantage estimator*, which is based on a *1-step* return estimation given by

$$\hat{A}(C, g, x) = r(C, g, x) + \gamma \left(\max_{g' \in IG(\ell, C, g, x)} V^{\pi_x}(C', g') \right) - V^{\pi_x}(C, g), \quad (6)$$

where $r(C, g, x)$ is the reward of applying transformation x to gate g of circuit C , C' denotes the new circuit obtained by applying the transformation, and $IG(\ell, C, g, x)$ is the ℓ -hop influenced gates of this transformation (defined below) to ensure locality.

DEFINITION 2 (ℓ -HOP INFLUENCED GATES). For a transformation x applied at gate g of circuit C , its ℓ -hop influenced gates, denoted $IG(\ell, C, g, x)$, is gate set of the new circuit C' that includes (1) all the new gates introduced by the transformation, and (2) all ℓ -hop (directed) predecessors of these gates.

$IG(\ell, C, g, x)$ includes all gates in the new circuit C' influenced by transformation x , which can fall two categories. First, all gates in the target graph of the transformation are in $IG(\ell, C, g, x)$, since these gates are newly introduced by the transformation. For transformation T_1 in Figure 5, g_0, g_1 , and g_2 are added to the new circuit by applying T_1 . Second, $IG(\ell, C, g, x)$ also includes gates whose applicable transformations may change due to the transformation. For this category, we consider all ℓ -hop predecessors of the new gates. Figure 5 shows the 1- and 2-hop influenced gates. Quarl locates a transformation based on a topologically minimal gate in the source graph of the transformation. Therefore for any gate not influenced by a transformation x , its applicable transformations remain the same after applying transformation x , as shown in Theorem 1.

THEOREM 1 (PROPERTY OF INFLUENCED GATES). Let C' be the new circuit obtained by applying transformation x to gate g on circuit C , and assume that for any transformation (G, G') the depth of G is at most d (the depth of a directed acyclic graph is the maximal length of a path in the graph). For any gate $g', g' \in C' \wedge g' \notin IG(d, C, g, x)$, its set of applicable transformations is identical in C and C' .

PROOF. See supplementary material. □

Quarl uses influenced gates to capture dependencies between transformations when estimating their advantages. As per eq. (6), Quarl estimates the local advantage of a transformation based on the maximum V^{π_x} (calculated by the gate value predictor) across all influenced gates of the transformation. The rationale behind the *max* aggregator is to propagate the reward signal through the dependency path of transformations, so our hierarchical advantage estimator can capture the rewards that truly depend on the current transformation. In our experiments, the maximal depth of circuits used in transformations is 4, but in practice we found that using 1-hop influenced gates leads to better results than using 4-hop influenced gates suggested by Theorem 1. We note that while

some transformations have a depth of 4, most have a lower depth; including more predecessors introduces more variance into the training process as the value of the maximal-value node in the influenced gates may not always be related to the applied transformation.

5.2 Training Data Collection

Generating Trajectories. As shown in Algorithm 1 line 5-19, in each training iteration, Quarl generates a total of B trajectories according to the current policy, and each trajectory is limited to at most T steps. These generated trajectories are taken as the training dataset to update the gate-and transformation-selecting policies. To generate the j -th trajectory, Quarl randomly selects an initial circuit $C_0^{(j)}$ from the *initial circuit buffer* C (introduced later in this section), and iteratively applies transformations on the selected circuit. Specifically, at the t -th time step, Quarl takes the current circuit $C_{t-1}^{(j)}$ as an input and chooses a gate $g_t^{(j)}$ and a transformation $x_t^{(j)}$ using the gate-and transformation-selecting policies. After that, $x_t^{(j)}$ is applied to $g_t^{(j)}$ on $C_{t-1}^{(j)}$ to generate a new circuit $C_t^{(j)}$. At each time step, Quarl collects the following data: (1) the current and new circuits $C_{t-1}^{(j)}$ and $C_t^{(j)}$, (2) the selected action $(g_t^{(j)}, x_t^{(j)})$, (3) the immediate reward r_t , (4) the value of $g_t^{(j)}$ given by the gate value predictor $V^{\pi_x}(C_{t-1}^{(j)}, g_t^{(j)}; \theta_g)$ (see Section 4.2), and (5) the probability of choosing $x_t^{(j)}$ under the current transformation-selecting policy (i.e., $\pi_x(x_t^{(j)}|C_{t-1}^{(j)}, g_t^{(j)}; \theta_x)$). The collected data is saved in a *rollout buffer* \mathcal{R} , which is initialized to empty at the start of each iteration.

Stop conditions. After a trajectory begins, Quarl keeps applying transformations on the current circuit until one of the following stop conditions is satisfied. First, each trajectory can have at most T time steps, where T is a hyper-parameter. Second, Quarl introduces a special transformation named NOP into the transformation set. Selecting NOP as the transformation (Algorithm 1 line 18) indicates that Quarl chooses to end the current trajectory, which provides Quarl the ability to stop when it finds that moving forward cannot bring benefits or even leads to negative rewards. Third, Quarl stops the current trajectory when the cost of the current circuit is α times greater than the cost of the input circuit (Algorithm 1 line 18), which prevents Quarl from moving toward a wrong direction too far. We set α to be 1.2 in our evaluation.

Initial circuit buffer. Instead of always starting from the input circuit C_{input} in a trajectory, Quarl samples a circuit from an *initial circuit buffer* C (Algorithm 1 line 16-17). C includes all circuits discovered in previous trajectories whose cost is lower than the trajectory’s initial circuit. C is a hash map with keys being the cost and values being the set of circuits with that cost. To select a circuit from C , Quarl first samples cost and then uniformly selects a circuit from the set of circuits with the sampled cost. Users can define customized probability distributions over costs depending on how they expect their agent to behave. Specifically, a greedier distribution where probabilities for sampling lower costs are larger makes the agent more progressive in doing optimization, preferring to extend lower-cost states.

Compared to always starting a trajectory from C_{input} , sampling circuits from the initial circuit buffer enhances the exploration of the search space. In particular, starting from C_{input} restricts Quarl to only explore circuits at most T steps away from C_{input} , where T is the maximum number of steps in a trajectory. In contrast, starting from a randomly selected circuit allows Quarl to explore previously unknown areas, enabling Quarl to discover more optimized circuits.

5.3 Agent Update

To update Quarl’s neural architecture, we first traverse the rollout buffer, and compute the advantage value for each time step according to eq. (6). Next, we train the graph embedding network, the

node reward predictor network and the transformation selector network jointly with stochastic gradient descent for M epochs. Following the PPO algorithm in eq. (1), the loss function for the transformation selector can be rewritten as

$$L^{TS}(\theta_x) = E_\tau \left[\sum_t \min(\rho_t(\theta_x)\hat{A}_t, \text{clip}(\rho_t(\theta_x), \epsilon)\hat{A}_t) \right] \quad (7)$$

where $\rho_t(\theta_x) = \frac{\pi_x(x_t|C_t, g_t; \theta_x)}{\pi_x(x_t|C_t, g_t; \theta_x(\text{old}))}$. To update the value estimator network, which is also the gate selecting policy, Quarl minimizes $L^{VE}(\theta_g)$ given by

$$L^{VE}(\theta_g) = E_\tau \left[\sum_t \hat{A}(C_t, g_t, x_t)^2 \right] \quad (8)$$

To train the networks jointly, we combine these loss functions into

$$L(\theta) = L^{TS}(\theta_x) + c_1 L^{VE}(\theta_g) + c_2 H(\pi_x; \theta_x) \quad (9)$$

where θ denotes all the trainable parameters combining θ_g and θ_x , $c_1 \geq 0$ and $c_2 \geq 0$ are two coefficients, and $H(\pi_x)$ denotes the entropy of policy π_x , which serves as a regularization term to promote exploration.

5.4 Pre-training, Fine-tuning, and Policy-guided Search

Circuits implemented in the same gate set share common local topologies, which offers opportunities to transfer the learned optimizations from one circuit to another in the same gate set. This observation motivates our pre-training and fine-tuning approach through which we can avoid training from scratch on previously unseen circuits and accelerate training. As introduced in Section 4, Quarl’s neural architecture can automatically adapt to circuits with different sizes and/or topologies, which enables the pre-training and fine-tuning pipeline.

Pre-training. The goal of the pre-training phase is to help the agent learn how to optimize different local structures. Quarl uses a diversity of circuits for pre-training, which allows the agent to explore various local structures and prevents over-fitting to the structure of a single circuit. Minor changes are needed to support training Quarl on multiple circuits. In the initial buffer, circuits are clustered into equivalent groups. At the beginning of each trajectory, Quarl chooses the initial circuit of a trajectory by first uniformly sampling an equivalent group and then randomly selecting a circuit from the group. All trajectories are used in gradient estimations to update the agent.

Fine-tuning. Quarl optimizes a new circuit by fine-tuning the pre-trained model on the circuit, which allows Quarl to discover optimizations specific to the new circuit. During the fine-tuning, there is a single equivalent group in the initial buffer, which corresponds to the new circuit Quarl fine-tunes on. Optimized circuits may be discovered during the fine-tuning, however, the primary goal of fine-tuning is to make the agent fit to the new circuit, specifically, the model should learn the gate values and policy distribution specific to the new circuit. Once the model has fitted to the new circuit, we should stop the fine-tuning to avoid wasting computation and use the fine-tuned model to apply a more efficient *policy-guided search* to finish the rest of the optimization.

Policy-guided search. In this stage, we employ a circuit optimization model that has been fitted to the circuit at hand. We use this model to guide the further optimization of the circuit using a technique we call *policy-guided search*, which shares some similarities with the trajectory collection stage during training. However, there are a few key differences between policy-guided search and trajectory collection. First, policy-guided search only maintains circuits with lowest cost in the initial circuit buffer, ensuring that Quarl uses one of the best discovered circuits to start a trajectory.

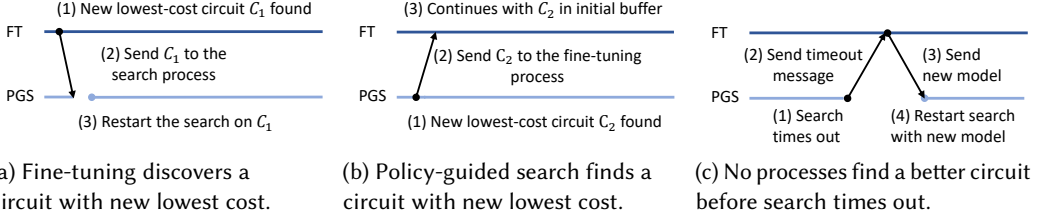


Fig. 6. Interactions between Quarl’s fine-tuning (FT) and policy-guided search (PGS) processes. (a) and (b) show how the two processes exchange information when a circuit with new lowest cost is discovered. (c) shows the case where the policy-guided search times out.

Second, after selecting a gate using the gate-selecting policy, instead of sampling a transformation from the transformation-selecting policy, Quarl selects the transformation with highest probability. During the search, if the transformation-selecting policy triggers a stop condition (described in Section 5.2) when select a transformation for a gate g on circuit C , Quarl applies a *hard mask* to g , which will prevent Quarl from revisiting g . Furthermore, to prevent Quarl from exploiting the policy without exploration, we also apply *soft masks* to gates that have been visited by Quarl for at least once. The difference between hard and soft masks is that once all gates in a circuit have been masked out, either by hard or soft masks, we remove the soft masks and do not reapply them. The purpose of soft masks is to ensure that every gate in a circuit C is visited at least once if the circuit is visited at least $|C|$ times. Whenever a circuit with lower cost is discovered, Quarl clears the initial circuit buffer, adds the circuit to the initial circuit buffer, and restarts the search.

Optimizing a circuit. To optimize an input circuit, Quarl runs a fine-tuning process and a policy-guided search process simultaneously. Figure 6 shows the interactions between the two processes, which exchange information whenever one process discovers a circuit with new lowest cost. Specifically, if a circuit C_1 with new lowest cost is found during fine-tuning, Quarl restarts the search using C_1 , as shown in Figure 6a. Conversely, if a circuit C_2 with new lowest cost is found during the search, the fine-tuning process will include C_2 in its initial circuit buffer and continue fine-tuning, as shown in Figure 6b. Moreover, a timeout is set for the search process in case that its model is obsolete. If no new lowest cost circuit is discovered before timeout, Quarl restarts the policy-guided search using the most recently model from fine-tuning, as shown in Figure 6c.

5.5 Scaling to Large Circuits

This section analyzes the scalability of Quarl during the training data collection and agent update phases, and describe how we improve its scalability for larger circuits.

Scalability of training data collection. To optimize an input circuit C , Quarl’s gate value predictor computes a value for every gate in C at each step in a trajectory. This process consists of a GNN inference to generate the representation of all gates in C , and an MLP inference that calculates the values of C ’s gates. For each gate, both the GNN and MLP inferences take constant time, therefore the overall time complexity of the gate selector is $O(|C|)$. After a gate g is selected, selecting a transformation and identifying the l -hop influenced gates takes constant time. Overall, the time complexity of Quarl’s data collection is $O(|C|)$.

However, as the size of the circuit grows, a significant amount of computation is discarded since all but one gate’s representation are not used after gate selection. To address this inefficiency, Quarl partitions an input circuit into sub-circuits by limiting the number of gates in each sub-circuit, and optimize these sub-circuits individually. This approach reduces the cost of training data collection to a constant. We evaluate the performance improvement of circuit partitioning in Section 6.6.

However, partitioning circuits may lead to missed optimization opportunities that span across partitions, which we plan to explore in future work.

Scalability of agent update. The agent update phase involves recomputing the probability of choosing the same transformation in the data collection phase. Specifically, to calculate the importance sampling ratio $\rho_t(\theta_x)$ in the loss function (Equation (7)), we need the probability $\pi_x(x_t|C_t, g_t; \theta_x)$ under the updated θ_x . Since π_x is based on the gate representation, which is also changed due to the update to the parameters of the GNN. As a result, Quarl needs to re-calculate the representation for g_t , which takes $O(|C_t|)$. Also, the network update phase involves gradient computation and backward-propagation, whose peak GPU memory usage is $O(|C_t|)$. On GPUs with limited device memory, we hand-tune the training batch-size to prevent out-of-memory issues.

Again, only a small number of gates are involved in the gradient generation, while the representation of other gates are compute-to-discard. We deal with this issue based on the fact that since the gate representation only contains information of its k -hop neighborhood, we can obtain exactly the same representation by running GNN only on its k -hop neighborhood. The number of gates in the k -hop neighborhood of a gate has a constant upper bound due to the sparse structure of quantum circuits. With this optimization, the complexity of computing gradient on a single data point becomes a constant.

Note that due to the design of Quarl’s neural architecture, the time and space complexity of Quarl only depend the number of gates in a circuit, rather than the number of qubits.

6 EVALUATION

We include the implementation details and evaluate Quarl in this section. Section 6.1 introduces the experimental setups and Section 6.2 describes the implementation of Quarl and hyperparameters. Section 6.3 and Section 6.4 shows the comparison of Quarl with existing optimizers on the Nam gate set and the IBM gate set, respectively. Section 6.6 focuses on evaluating Quarl’s scalability, and Section 6.5 performs a comprehensive ablation study.

6.1 Experimental Setup

Benchmarks. To evaluate the effectiveness of our framework, we employ a widely-adopted quantum circuit benchmark suite, which has been previously used by several works (Amy et al., 2014, Hietala et al., 2021, Kissinger and van de Wetering, 2020, Nam et al., 2018, Xu et al., 2022b) for logical circuit optimization. The benchmark suite primarily comprises arithmetic and reversible circuits, and we evaluate them in the Nam gate set (CX, Rz, H, X), following existing studies. Additionally, we transpile these benchmark circuits to the IBM gate set ($\{CX, Rz, X, SX\}$) to demonstrate Quarl’s compatibility with different gate sets. Since this benchmark suite contains a limited number of circuit types, we extend our evaluation to include circuits from the MQTBench library (Quetschlich et al., 2022), which encompasses circuits from various categories, such as QAOA (Farhi et al., 2014) and VQE (Peruzzo et al., 2014b).

Metrics. We use four metrics in our evaluation: total gate count, CNOT count, circuit depth, and fidelity. Operations on NISQ devices are affected by noise, and the error rates of different gates vary. Specifically, the error rate of two-qubit gates (e.g. CNOT) are typically an order of magnitude larger than single-qubit gates (e.g., 3×10^{-2} and 4.43×10^{-3} , respectively, on IBM Q20 (Li et al., 2018)). In light of this, we evaluate Quarl with not only total gate count but also CNOT count. Moreover, since qubits in NISQ devices have limited coherence time, circuit depth should be within a certain range for successful execution. The optimizing results ultimately translate to the fidelity of executions. However, the end-to-end fidelity involves many factors, such as mapping method, routing method, device coupling map and device error rate, which are out of the scope of logical

circuit optimization. To rule out the effect of these factors, we follow prior work (Xu et al., 2022a) and report the absolute circuit fidelity, which is defined as the product of the success rate of all gates in the circuit. For a circuit C , its fidelity can be expressed as $\prod_{g \in C} (1 - e(g))$ where $e(g)$ denotes the empirical device error rate for gate g . During evaluation, we use the calibration data of IBM Washington device (IBM, 2023) where CNOT error rate is 1.214×10^{-2} , Rz error rate is 0, and the error rate of other single-qubit gates (i.e. X gate and SX gate) are 2.77×10^{-4} .

Server specification. Our experiments are conducted on the Perlmutter supercomputer (per, 2023). Pre-training is performed on a node equipped with an AMD EPYC 7763 64-core 128-thread processor, 256GB DRAM, and four NVIDIA A100-SXM4-40GB GPUs. For circuit optimization, we use a node with the same hardware specification, but with only one NVIDIA A100-SXM4-40GB GPU.

6.2 Implementation Details

We build the Quarl training pipeline on top of PyTorch (Paszke et al., 2019) and DGL (Wang et al., 2019b). We utilize the APIs provided by Quartz (Xu et al., 2022c) to generate graph representations of circuits and transformation rules and perform graph pattern matching. These APIs are encapsulated with Cython (Wang et al., 2019a) to facilitate their invocations by Python processes.

Data-parallel pre-training. During pre-training, Quarl employs a distributed data-parallel pipeline to train its neural architecture across multiple GPUs. Specifically, each process occupies a single GPU and contains an independent agent that takes actions to collect trajectories and compute gradients using the collected data. At the end of each training iteration, Quarl synchronizes the gradients across all GPUs to update the model parameters. Each process maintains an individual initial circuit buffer and exchanges information about the lowest-cost circuits with each other. In the experiments, for each gate set, we pre-train Quarl’s neural architecture on six circuits (i.e. barenco_tof_3, gf2^4_mult, mod5_4, mod_mult_55, tof_5, and vbe_adder_3) for 8 hours with 4 GPUs. We choose these circuits for pre-training because they are relatively small and have diverse circuit topologies. Since the pre-trained models are reused in circuit optimization, we do not count the pre-training time when reporting Quarl’s search time.

Table 1. Hyperparameters used in Quarl’s training.

Hyperparameter	Pre-training	Fine-tuning
Horizon (T)	600	600
Actor learning rate	3e-4	3e-4
Critic learning rate	5e-4	5e-4
GNN learning rate	3e-4	3e-4
Num. actors	128	64
Num. epochs	20	5
Minibatch size	4800	4800
Discount (γ)	0.95	0.95
Clipping parameter ϵ	0.2	0.2
Entropy coeff.	0.02	0.02

Fine-tuning and policy-guided search. In the experiment, the fine-tuning process starts 5 minutes earlier than the search process, allowing Quarl’s neural architectures to learn to discover circuit-specific optimizations before starting the search. The search timeout is set to 20 minutes. We run Quarl for 6 hours on each input circuit.

Rotation merging. Aside from circuit transformations, many quantum circuit optimizers, including Nam (Nam et al., 2018), VOQC (Hietala et al., 2021) and Quartz (Xu et al., 2022c), incorporate *rotation merging*, a technique that merges R_z gates with identical phase polynomial expressions (Nam et al., 2018), into their optimization pipeline. However, the R_z gates being merged may be arbitrarily far apart, making it difficult to represent rotation merging as combinations of local circuit transformations. To address this challenge, we integrate rotation merging into Quarl’s circuit transformation process, following prior work. Figure 7b demonstrates that Quarl can autonomously identify optimizations similar to rotation merging through its own exploration of certain circuits.

Table 2. Comparing Quarl and existing circuit optimizers on reducing total gate count of the benchmark circuits for the Nam gate set. The best result for each circuit is in bold.

Circuit	Total Gate Count (Nam gate set)								
	Orig.	Nam	VOQC	Qiskit	Tket	Quartz w/ R.M.	Quartz w/o R.M.	Quarl w/ R.M.	Quarl w/o R.M.
tof_3	45	35	35	43	39	35	35	33	33
barenco_tof_3	58	40	40	54	49	40	46	35	36
mod5_4	63	51	51	61	57	37	39	24	24
tof_4	75	55	55	71	64	55	55	51	51
barenco_tof_4	114	72	72	106	97	72	90	62	62
tof_5	105	75	75	99	89	75	75	69	69
mod_mult_55	119	91	92	115	103	90	94	84	84
vbe_adder_3	150	89	89	189	130	89	112	71	71
barenco_tof_5	170	104	104	158	145	104	134	90	96
csla_mux_3	170	155	158	249	149	148	146	141	141
rc_adder_6	200	140	152	226	172	152	170	134	148
gf2^4_mult	225	187	186	212	205	176	215	160	163
tof_10	255	175	175	239	214	175	175	169	169
mod_red_21	278	180	184	256	223	198	268	179	177
hwb6	259	-	209	258	217	214	250	193	196
gf2^5_mult	347	296	287	327	319	274	334	257	266
csum_mux_9	420	266	280	420	365	256	420	224	282
barenco_tof_10	450	264	264	418	385	264	450	236	274
qcla_com_7	443	284	269	498	377	288	431	258	277
ham15-low	443	-	348	421	392	360	435	323	322
gf2^6_mult	495	403	401	464	453	391	485	352	386
qcla_adder_10	521	399	416	630	444	404	518	380	391
gf2^7_mult	669	555	543	627	614	531	657	484	530
gf2^8_mult	883	712	706	819	806	703	883	648	755
qcla_mod_7	884	624	678	933	759	652	884	629	664
adder_8	900	606	596	1001	802	624	874	560	669
Geo. Mean Reduction	-	28.0%	27.0%	-0.6%	13.1%	28.3%	12.9%	35.8%	32.6%

Cost function. In all our experiments, we use total gate count as the cost function for Quarl. While 2-qubit gate count (e.g., CNOT count) can also be used as the cost function, we find that both of them yield equally good results in 2-qubit gate count. However, in some scenarios, minimizing the count of a specific type of 1-qubit gate is crucial. For example, minimizing the count of Rz gates is essential in fault-tolerant quantum computing settings, as Rz is non-Clifford and is more expensive to implement than Clifford gates in error correction. Thus, we select total gate count as the cost function. We do not adopt fidelity as the cost function because, at the logical optimization layer, we lack hardware specification, and the circuit is not physically mapped or routed.

Hyperparameters. In our evaluation, Quarl uses a 6-layer graph neural network (GNN) as the gate representation generator, with a hidden dimension size of 128. The gate selector and the transformation selector are both two-layer multiple layer perceptron (MLP) with a hidden dimension size of 128 and 256, respectively. Table 1 lists the hyperparameters used in Quarl’s learning process. We choose $\lambda = 0.9$ in Quarl’s gate selector and use 1-hop influenced gates in training.

6.3 Comparison on the Nam Gate Set

We compare Quarl with existing rule-based ¹ (i.e. Nam (Nam et al., 2018), VOQC (Hietala et al., 2021), Qiskit (Aleksandrowicz et al., 2019) and t|ket) (Sivarajah et al., 2020)) and search-based ² (i.e. Quartz (Xu et al., 2022c)) optimizers on total gate count, CNOT count, and circuit depth on

¹PyZX (Kissinger and van de Wetering, 2020) is another rule-based optimizer. However, it only minimizes the T gate count and does not explicitly optimize our chosen metrics, namely total gate count, CNOT count, circuit fidelity, and depth. We observe that PyZX achieves worse performance on these metrics and therefore exclude it in this comparison.

²QUESO (Xu et al., 2022a) is another search-based optimizer. It is not publicly available yet, which prevents us from conducting a comparison. We plan to include it in the final paper if it is open source later.

Table 3. Comparing Quarl and existing circuit optimizers on reducing CNOT count of the benchmark circuits for the Nam gate set. The best result for each circuit is in bold.

Circuit	CNOT Count (Nam gate set)								
	Orig.	Nam	VOQC	Qiskit	Tket	Quartz w/ R.M.	Quartz w/o R.M.	Quarl w/ R.M.	Quarl w/o R.M.
tof_3	18	14	14	18	18	14	14	12	12
barenco_tof_3	24	18	18	24	24	18	20	13	14
mod5_4	28	28	28	28	28	20	22	13	13
tof_4	30	22	22	30	30	22	22	18	18
barenco_tof_4	48	48	34	48	48	34	40	24	24
tof_5	42	30	30	42	42	30	30	24	24
mod_mult_55	48	40	42	48	48	39	41	37	36
vbe_adder_3	70	50	50	62	62	44	50	32	32
barenco_tof_5	72	50	50	72	72	50	60	36	42
cs1a_mux_3	80	70	74	71	71	70	68	63	63
rc_adder_6	93	71	71	81	81	71	77	61	67
gf2^4_mult	99	99	99	99	99	95	99	79	81
tof_10	102	70	70	102	102	70	70	64	64
mod_red_21	105	81	81	105	104	81	105	74	74
hwb6	116	-	104	115	111	99	115	86	88
gf2^5_mult	154	154	154	154	154	149	154	132	133
csum_mux_9	168	140	140	168	168	140	168	112	140
barenco_tof_10	192	130	130	192	192	130	192	102	122
qcla_com_7	186	132	132	174	174	127	178	111	120
ham15-low	236	-	210	236	225	209	236	185	180
gf2^6_mult	221	221	221	221	221	221	221	182	197
qcla_adder_10	233	183	199	213	205	187	230	165	169
gf2^7_mult	300	300	300	300	300	300	300	253	271
gf2^8_mult	405	405	405	405	402	405	405	364	393
qcla_mod_7	382	292	328	366	366	307	382	285	296
adder_8	409	291	301	385	383	305	395	265	313
Geo. Mean Reduction	-	18.4%	17.8%	2.5%	3.0%	20.6%	10.9%	33.9%	30.7%

the Nam gate set. We did evaluate on circuit fidelity since the Nam gate set is not hardware native. Both Quarl and Quartz (Xu et al., 2022c) use a set of 6206 transformation rules generated by Quartz. This section (and Section 6.4) focus on circuits with less than 1,500 gates, and Section 6.6 evaluates the performance and scalability of Quarl on larger circuits. Nam et al. (2018) and VOQC (Hietala et al., 2021) have both incorporated rotation merging into their framework while Quartz adopts it as a preprocessing procedure. Similarly, Quarl adopts rotation merging as a preprocessing step. However, to demonstrate the effectiveness of Quarl without rotation merging, we report results of both Quarl and Quartz without rotation merging.

As shown in Table 2, Quarl outperforms existing rule-based circuit optimizers on almost all benchmark circuits. Rule-based optimizers rely on a fixed set of manually designed rules and schedule them in a predetermined, typically greedy, manner. For instance, Nam (Nam et al., 2018) is an optimizer that has been specifically fine-tuned for the Nam gate set and is among the best-performing rule-based optimizers on that gate set. Nam applies gate-set-specific heuristics and rules, such as rotation merging and floating R_z gates, and also uses 1- and 2-qubit gate cancellation as subroutines to simplify the circuits. To apply these subroutines, Nam et al. (2018) uses two fixed schedules. We report the results of the *heavy* schedule, which applies more aggressive optimization and achieves better results. Other rule-based optimizers (i.e., VOQC (Hietala et al., 2021), Qiskit (Aleksandrowicz et al., 2019), tket) (Sivarajah et al., 2020)) operate similarly, where VOQC (Hietala et al., 2021) also implements specific optimizations for the Nam gate set, which are combined into a pass `optimize_nam`. In contrast, Quarl is equipped with transformation rules automatically generated by Quartz (Xu et al., 2022c).

Quarl surpasses Quartz (Xu et al., 2022c) for *all* benchmark circuits. Both tools employ the same set of transformations, and therefore the difference in their performance arises from their respective

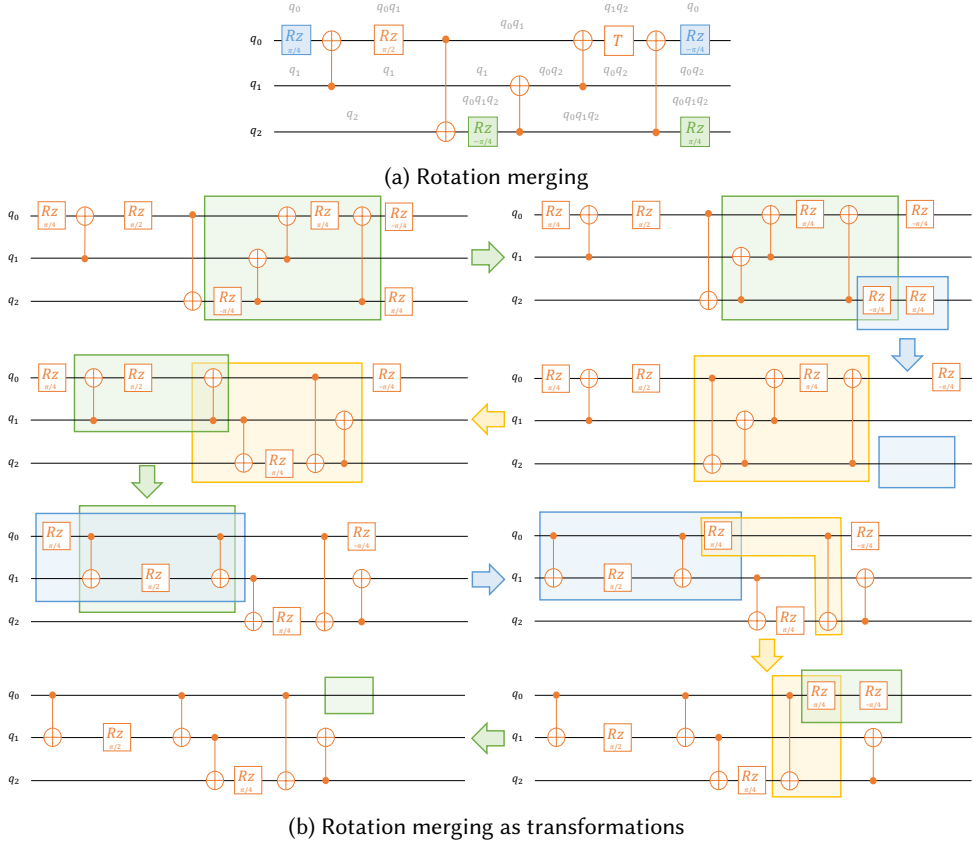


Fig. 7. (a) shows an example circuit with CNOT and Rz gates. The phase of each Rz gate is shown above the gate. Rotations with identical phase can be combined by rotation merging. (b) represents the rotation merging optimization as a sequence of transformations discovered by Quarl. Note that Quarl can also update the final circuit to have the same CNOT topology as the original circuit by applying a few additional transformations, which are omitted in the figure.

search algorithms. Quartz uses cost-based backtracking search to schedule transformations, while Quarl leverages reinforcement learning to detect optimization opportunities and determine the best combination of transformations to achieve them.

The reduction in gate count achieved by Quarl translates to an average reduction of 25.7% in circuit depth, which outperforms the best depth reduction achieved by existing optimizers (i.e., 19.6%). We report the circuit depth results in the supplementary material due to the page limit.

Table 3 shows CNOT count reduction on the same gate set. Quarl reduces CNOT count by 33.9% on average, while the reduction achieves by existing optimizers is at most 20.6%. Reducing CNOT count is a desirable advantage since it significantly increases the fidelity of executing a circuit on modern NISQ devices with sparse inter-qubit connections. Even for relatively small circuits, Quarl achieves better performance than Quartz (Xu et al., 2022c), as shown in Table 2 and Table 3. This is because exhaustively exploring the search space is prohibitively expensive even for very small circuits, and Quartz’s back-tracking search discards circuits whose cost is larger than a threshold. This approach can miss optimizations that require applying cost-increasing transformations. In contrast, Quarl’s learning-based approach provides a more efficient and scalable solution, which allows Quarl to better explore the search space and discover more optimization opportunities.

Table 4. Comparing Quarl and existing circuit optimizers on reducing total gate count and CNOT count of the benchmark circuits for the IBM gate set. The best result for each circuit is in bold.

Circuit	Orig.		Qiskit		Tket		Quartz		Quarl	
	# gates	# CXs	# gates	# CXs	# gates	# CXs	# gates	# CXs	# gates	# CXs
tof_3	53	18	51	18	51	18	42	14	39	14
barenco_tof_3	65	24	61	24	61	24	52	20	42	16
mod5_4	71	28	69	28	69	28	62	27	50	22
tof_4	88	30	84	30	84	30	67	22	62	22
tof_5	123	42	117	42	117	42	92	30	85	30
barenco_tof_4	125	48	117	48	117	48	99	40	75	30
mod_mult_55	140	48	135	48	145	48	114	41	100	39
vbe_adder_3	165	70	186	62	159	62	124	50	82	36
barenco_tof_5	185	72	173	72	173	72	146	60	108	44
cs1a_mux_3	200	80	235	71	188	71	181	72	164	65
rc_adder_6	229	93	250	81	277	81	189	75	164	71
gf2^4_mult	246	99	232	99	232	99	229	99	192	84
hwb6	287	116	281	115	282	111	272	114	208	85
mod_red_21	294	105	279	105	317	104	292	105	204	77
tof_10	298	102	282	102	282	102	217	70	203	70
gf2^5_mult	374	154	353	154	353	154	372	154	295	135
csum_mux_9	459	168	453	168	474	168	459	168	318	140
barenco_tof_10	485	192	453	192	453	192	482	192	278	116
ham15-low	485	236	456	236	455	225	480	234	366	188
qcla_com_7	486	186	511	174	486	174	470	174	304	119
gf2^6_mult	528	221	496	221	496	221	528	221	422	198
qcla_adder_10	587	233	636	213	556	205	586	232	412	164
gf2^7_mult	708	300	665	300	665	300	708	300	573	273
gf2^8_mult	928	405	864	405	861	402	923	403	821	392
qcla_mod_7	982	382	980	366	933	366	978	382	746	308
adder_8	1004	409	1010	385	1169	383	997	405	685	283
vqe_8	199	14	91	14	93	14	92	14	89	14
qgan_8	256	28	114	28	98	28	100	26	81	18
qaoa_8	284	32	211	32	159	32	157	32	163	32
ae_8	502	56	350	56	283	56	373	56	305	56
qpeexact_8	555	64	373	64	286	55	371	64	326	63
qpeinexact_8	571	65	381	65	312	56	381	65	332	65
qft_8	578	68	392	68	262	56	326	67	298	67
qftentangled_8	647	75	415	75	295	61	489	75	332	75
portfoliovqe_8	708	84	288	84	232	84	359	84	202	54
portfolioqaoa_8	1352	168	975	168	712	168	1207	168	806	161
Geo. Mean Reduction	-	-	14.4%	1.8%	20.1%	4.1%	19.9%	7.7%	36.6%	21.3%

As shown in Table 2 and Table 3, the performance gap between Quarl with and without rotation merging is relatively small (i.e., 3.2% in both cases); as a comparison, disabling rotation merging decreases Quartz’s performance by 15.4% for total gate count and 9.7% for CNOT count. Rotation merging is an efficient global optimization technique that merges R_z gates with identical phase polynomial expressions. Though it can be achieved by multiple applications of local R_z transformation rules, it is challenging to rebuild rotation merging with those rules since applying them does not provide immediate rewards until we finally fuse the rotation gates. Though it takes some time to learn, once the best schedule is learned, Quarl can apply it every where, which is much more efficient. Quarl can learn to perform optimizations similar to rotation merging through its own exploration. Section 6.3 shows such an example, where Quarl merges two pairs of R_z gates with identical phase polynomial using a sequence of local transformations.

6.4 Comparison on the IBM Gate Set

We also conduct a comparison between Quarl and existing optimizers on the IBM gate set using four metrics: total gate count, CNOT count, circuit depth, and fidelity. To optimize a circuit, both Quarl and Quartz (Xu et al., 2022c) use a set of 6881 transformation rules generated by Quartz. For parametric quantum gates, Quartz only discovers symbolic transformations applicable to these

gates with arbitrary parameter values, and misses transformations that are only valid for specific parameter values. Some of these transformations missed by Quartz are important to optimize circuits on the IBM gate set. To address this limitation, we also include three single-qubit transformations missed by Quartz: (1) $Rz(\pi) = SX Rz(\pi) SX$, (2) $SX Rz(\pi/2) SX = Rz(\pi/2) SX Rz(\pi/2)$, and (3) $SX Rz(3\pi/2) SX = Rz(3\pi/2) SX Rz(3\pi/2)$. We verify their correctness by directly computing the concrete matrix representation of the two circuits in each transformation. These three transformations are used by both Quarl and Quartz to optimize circuits. Since rotation merging is not native to the IBM gate set, it is not applied during the evaluation.

As shown in Table 4, Quarl greatly outperform existing optimizers for the IBM gate set for both total gate count and CNOT count. Specifically, Quarl reduces total gate count by 36.6% on average, while existing optimizers reduce total gate count by at most 20.1%. The Quarl-optimized circuits also reduce CNOT count by 21.3%, while existing approaches can achieve up to 7.7% CNOT count reduction. The performance gap between Quarl and Quartz (Xu et al., 2022c) is widened on the IBM gate set. We hypothesize this is because of Quartz’s reliance on rotation merging as a preprocessing pass, which is not applicable on the IBM gate set. Quarl achieves 22.1% circuit depth reduction on average, whereas existing optimizers reduce the circuit depth by at most 13.5%. We report the circuit depth results in the supplementary material.

Figure 8 shows the fidelity improvement achieved by different optimizers. Quarl improves circuit fidelity by up to 4.66× (on adder_8) and 1.37 times on average, while Qiskit, Tket and Quartz improve circuit fidelity by 1.04×, 1.07×, 1.06× on average, respectively. Quarl achieves the best fidelity improvements for most circuits. This is largely because CNOT involves a much higher error rate than other gates, and Quarl performs the best on CNOT reduction.

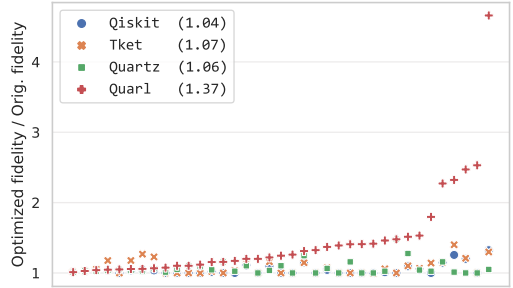


Fig. 8. Circuit fidelity comparison for the IBM gate set. The numbers in parentheses in the legend indicate the average relative fidelity improvement (geometric mean) achieved by the optimizers.

6.5 Ablation Studies

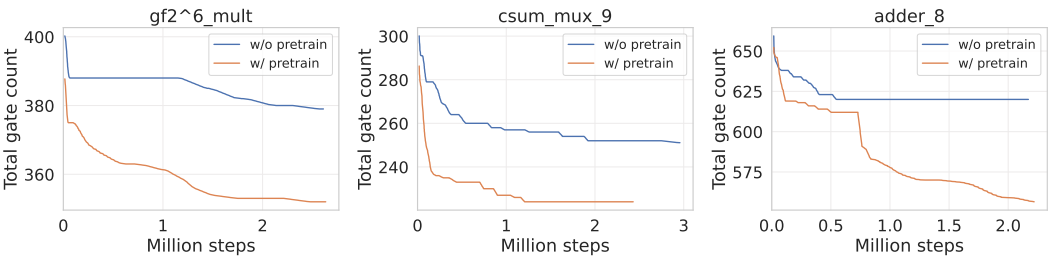


Fig. 9. Comparison on Quarl’s optimization with and without pretraining.

Pre-training. We evaluate whether Quarl’s pre-trained neural architecture can generalize to unseen circuits and how pre-training affects Quarl’s performance. We start a group of fine-tuning processes (with search) using the pre-trained model and another group of fine-tuning processes (with search) using randomly initialized parameters, and compare their performance. The results are shown in Figure 9. Note that these three circuits are much larger than the circuits used in

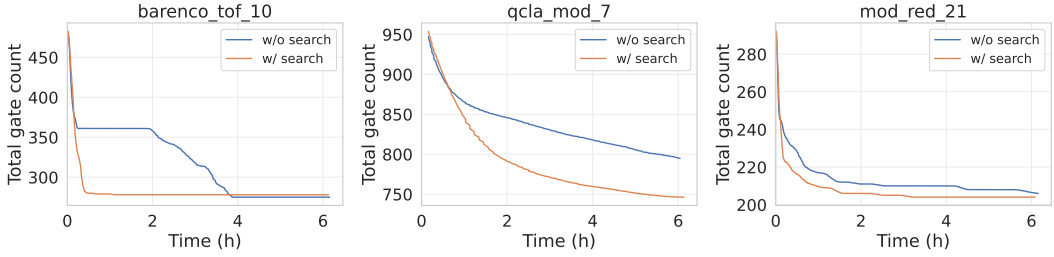


Fig. 10. Comparison on Quarl’s optimization with and without policy-guided search.

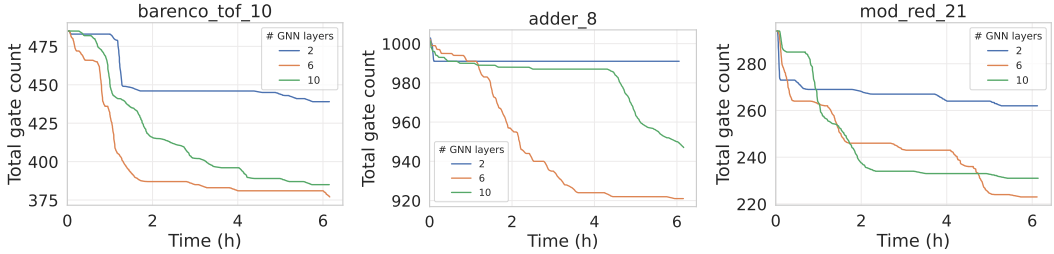


Fig. 11. Comparison on Quarl’s optimization with different GNN layers.

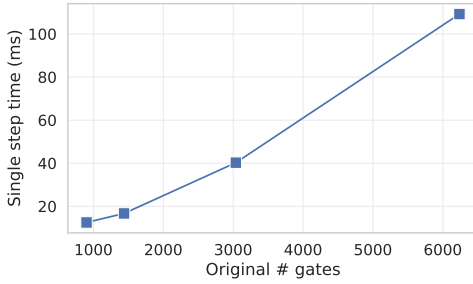
pre-training. Pre-training allows Quarl to quickly identify optimizations for all three circuits and eventually achieve better results, which shows that Quarl’s pre-trained model generalizes well to larger circuits and boosts optimization performance on previously unseen circuits.

Policy-guided search. To evaluate Quarl’s policy-guided search, we start two groups of experiments from the same pre-trained model checkpoint: the first group performs fine-tuning with policy-guided search while the second only conducts fine-tuning. As shown in Figure 10, policy-guided search allows Quarl to discover better solution faster. Compared to fine-tuning, Quarl’s policy-guided search allows greedier exploitation (i.e., storing only best cost circuits in the initial buffer and using argmax instead of sampling during transfer selection) and bolder exploration (i.e. using soft mask to force exploration).

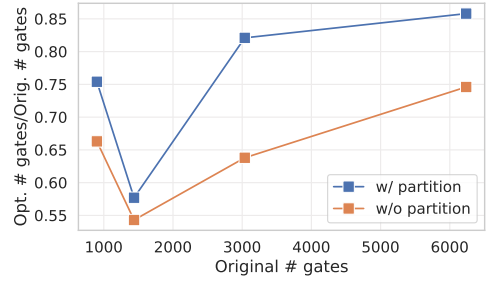
The number of GNN layers. An important hyperparameter in Quarl is the number of GNN layers in the gate representation generator (i.e., K in Section 4.1). Using more GNN layers allows Quarl to encode a larger subcircuit for each gate to guide the gate and transformation selection at the cost of introducing deeper network and more trainable parameters, which in turn requires more time and resource to train. Figure 11 shows Quarl’s performance with different values of K . We use randomly initialized model parameters to rule out the effect of pre-training, and train Quarl’s neural architecture with different values of K for 6 hours. Using a small value of K (e.g., $K = 2$) results in suboptimal performance, since Quarl’s gate and transformation selectors can only view a small neighborhood of each gate to make decision. A larger K enables representations to better guide the gate and transformation selection. However, a very large value of K (e.g., $K = 10$) is also suboptimal as it introduces more parameters which consumes more data to converge and increases the time cost of Quarl’s representation generator to encode subcircuit into representation.

6.6 Scalability Analysis

This section investigates the relationship between circuit size and time to collect training data, and evaluates how circuit partitioning improves Quarl’s scalability. We evaluate Quarl using four



(a) Relation between gate count and single-step time cost in data collection.



(b) Comparison between Quarl's performance with and without circuit partitioning.

Fig. 12. Scalability analysis.

circuits with similar structures, namely `adder_8`, `adder_16`, `adder_32`, and `adder_64`, which have 900, 1437, 3037, and 6237 gates, respectively. Figure 12a shows the time to collect training data for these circuits, which aligns well with our analysis in Section 5.5 and demonstrates a linear relation. Additionally, Figure 12b compares the performance of Quarl on the original and partitioned circuits, where we partition the input circuit into subcircuits with at most 512 gates based on a topological order. The experiments were conducted on the same computation platform with a search time budget of 2 hours to ensure a fair comparison and rule out the influence of optimization saturation. The results indicate that circuit partitioning generally increases Quarl's performance in limited search time, but it may lead to performance degradation due to missed optimization opportunities across partitions.

7 RELATED WORK

Quantum circuit optimization. In recent years, several optimizing compilers for quantum circuits have been introduced, such as Qiskit (Aleksandrowicz et al., 2019), t|ket> (Sivarajah et al., 2020), Quilc (Skilbeck et al., 2020), and voqc (Hietala et al., 2021). These optimizers rely on a rule-based strategy that applies manually designed circuit transformations whenever possible. Quartz (Xu et al., 2022c) uses a search-based approach that generates a comprehensive set of circuit transformations and applies them using a backtracking search algorithm. QUESO (Xu et al., 2022a), on the other hand, uses a path-sum-based approach to synthesize non-local circuit transformations and apply them using beam search. However, the large search space of functionally equivalent circuits and the need for cost-increasing transformations pose challenges for existing approaches to effectively discover circuit optimizations. Quarl addresses this challenge with a novel neural architecture and RL-training procedure, enabling it to automatically identify optimization opportunities and apply the right transformations through interaction with the environment. Different from the aforementioned compilers that apply transformations, PyZX (Kissinger and van de Wetering, 2020) represents circuits as ZX-diagrams and use ZX-calculus (Hadzihasanovic et al., 2018, Jeandel et al., 2018) to simplify ZX-diagrams, which are eventually converted back to the circuit representation. In contrast, Quarl is designed to learn to perform transformations. Applying Quarl's techniques to optimize circuits in ZX-calculus is a promising avenue for future research.

Reinforcement learning for quantum computing. Reinforcement learning has been applied to optimize quantum circuits. For instance, Ostaszewski et al. (2021) used Double Deep Q-Learning to optimize Variational Quantum Eigensolvers (VQEs) (Peruzzo et al., 2014a). Similarly, Fösel et al. (2021) utilized a convolutional neural network and PPO (Schulman et al., 2017) to learn circuit

transformations. However, this approach is limited to a small set of transformations with up to two qubits. Notably, Quarl differs from these methods in its ability to support a comprehensive set of thousands of transformations and optimize arbitrary quantum circuits.

Recently, reinforcement learning has also been applied to the qubit routing problem, which involves inserting SWAP gates into the circuits to enable their execution on near-term intermediate-scale quantum (NISQ) devices (Li et al., 2018). Existing examples include QRoute (Sinha et al., 2022) and a DQN-based method proposed by Pozzi et al. (2020), both of which aim to minimize the final depth of circuits after qubit routing using RL. It is worth noting that Quarl’s techniques are orthogonal to RL-based qubit routing techniques, and combining them may lead to further improvements in circuit optimization on NISQ devices.

8 CONCLUSION

In this paper, we present Quarl, a learning-based quantum circuit optimizer. In Quarl’s hierarchical approach, circuits are optimized with a sequence of transformation applications where in each application a gate-selecting policy and a transformation-selecting policy are used to choose a gate and a transformation to apply on the selected gate, respectively. The two policies are trained jointly, with a single actor-critic architecture. To apply PPO in the training of this architecture, we propose hierarchical advantage estimation (HAE) as an novel advantage estimator. Experiment results show that Quarl significantly outperforming existing circuit optimizers.

ACKNOWLEDGEMENT

We thank Shinjae, Yoo and Mingkuan Xu for their helpful feedback. This work is supported by NSF awards CNS-2147909, CNS-2211882, and CNS-2239351, and research awards from Amazon, Google, and Meta. This research used resources of the National Energy Research Scientific Computing Center (NERSC), a U.S. Department of Energy Office of Science User Facility located at Lawrence Berkeley National Laboratory, operated under Contract No. DE-AC02-05CH11231 using NERSC award DDR-ERCAP0023403.

REFERENCES

- The perlmutter supercomputer. <https://docs.nersc.gov/systems/perlmutter/>, 2023.
- A. F. Agarap. Deep learning using rectified linear units (relu), 2018. URL <https://arxiv.org/abs/1803.08375>.
- G. Aleksandrowicz, T. Alexander, P. Barkoutsos, L. Bello, Y. Ben-Haim, D. Bucher, F. J. Cabrera-Hernández, J. Carballo-Franquis, A. Chen, C.-F. Chen, J. M. Chow, A. D. Córcoles-Gonzales, A. J. Cross, A. Cross, J. Cruz-Benito, C. Culver, S. D. L. P. González, E. D. L. Torre, D. Ding, E. Dumitrescu, I. Duran, P. Eendebak, M. Everitt, I. F. Sertage, A. Frisch, A. Fuhrer, J. Gambetta, B. G. Gago, J. Gomez-Mosquera, D. Greenberg, I. Hamamura, V. Havlicek, J. Hellmers, Łukasz Herok, H. Horii, S. Hu, T. Imamichi, T. Itoko, A. Javadi-Abhari, N. Kanazawa, A. Karazeev, K. Krsulich, P. Liu, Y. Luh, Y. Maeng, M. Marques, F. J. Martín-Fernández, D. T. McClure, D. McKay, S. Meesala, A. Mezzacapo, N. Moll, D. M. Rodríguez, G. Nannicini, P. Nation, P. Ollitrault, L. J. O’Riordan, H. Paik, J. Pérez, A. Phan, M. Pistoia, V. Prutyaynov, M. Reuter, J. Rice, A. R. Davila, R. H. P. Rudy, M. Ryu, N. Sathaye, C. Schnabel, E. Schoute, K. Setia, Y. Shi, A. Silva, Y. Siraichi, S. Sivarajah, J. A. Smolin, M. Soeken, H. Takahashi, I. Tavernelli, C. Taylor, P. Taylour, K. Trabing, M. Treinish, W. Turner, D. Vogt-Lee, C. Vuillot, J. A. Wildstrom, J. Wilson, E. Winston, C. Wood, S. Wood, S. Wörner, I. Y. Akhalwaya, and C. Zoufal. Qiskit: An Open-source Framework for Quantum Computing, Jan. 2019. URL <https://doi.org/10.5281/zenodo.2562111>.
- M. Amy, D. Maslov, and M. Mosca. Polynomial-time t-depth optimization of clifford+t circuits via matroid partitioning. *IEEE Transactions on Computer-Aided Design of Integrated Circuits and Systems*, 33(10):1476–1489, 2014. doi: 10.1109/TCAD.2014.2341953.
- J. Biamonte, P. Wittek, N. Pancotti, P. Rebentrost, N. Wiebe, and S. Lloyd. Quantum machine learning. *Nature*, 549(7671): 195–202, 2017.
- Y. Cao, J. Romero, J. P. Olson, M. Degroote, P. D. Johnson, M. Kieferová, I. D. Kivlichan, T. Menke, B. Peropadre, N. P. Sawaya, et al. Quantum chemistry in the age of quantum computing. *Chemical reviews*, 119(19):10856–10915, 2019.
- E. Farhi, J. Goldstone, and S. Gutmann. A quantum approximate optimization algorithm. *arXiv preprint arXiv:1411.4028*, 2014.

- T. Fösel, M. Y. Niu, F. Marquardt, and L. Li. Quantum circuit optimization with deep reinforcement learning. *arXiv preprint arXiv:2103.07585*, 2021.
- M. W. Gardner and S. Dorling. Artificial neural networks (the multilayer perceptron)—a review of applications in the atmospheric sciences. *Atmospheric environment*, 32(14-15):2627–2636, 1998.
- A. Hadzihasanovic, K. F. Ng, and Q. Wang. Two complete axiomatisations of pure-state qubit quantum computing. In *Proceedings of the 33rd Annual ACM/IEEE Symposium on Logic in Computer Science, LICS '18*, page 502–511, New York, NY, USA, 2018. Association for Computing Machinery. ISBN 9781450355834. doi: 10.1145/3209108.3209128. URL <https://doi.org/10.1145/3209108.3209128>.
- W. Hamilton, Z. Ying, and J. Leskovec. Inductive representation learning on large graphs. *Advances in neural information processing systems*, 30, 2017.
- Y.-L. He, X.-L. Zhang, W. Ao, and J. Z. Huang. Determining the optimal temperature parameter for softmax function in reinforcement learning. *Applied Soft Computing*, 70:80–85, 2018.
- K. Hietala, R. Rand, S.-H. Hung, X. Wu, and M. Hicks. A verified optimizer for quantum circuits. *Proc. ACM Program. Lang.*, 5(POPL), Jan. 2021. doi: 10.1145/3434318. URL <https://doi.org/10.1145/3434318>.
- G. E. Hinton. Learning translation invariant recognition in a massively parallel networks. In *International Conference on Parallel Architectures and Languages Europe*, pages 1–13. Springer, 1987.
- IBM. The ibm washington quantum device., 2023. URL <https://reversiblebenchmarks.github.io/>.
- E. Jeandel, S. Perdrix, and R. Vilmart. A complete axiomatisation of the zx-calculus for clifford+t quantum mechanics. In *Proceedings of the 33rd Annual ACM/IEEE Symposium on Logic in Computer Science, LICS '18*, page 559–568, New York, NY, USA, 2018. Association for Computing Machinery. ISBN 9781450355834. doi: 10.1145/3209108.3209131. URL <https://doi.org/10.1145/3209108.3209131>.
- A. Kissinger and J. van de Wetering. PyZX: Large scale automated diagrammatic reasoning. *Electronic Proceedings in Theoretical Computer Science*, 318:229–241, may 2020. doi: 10.4204/eptcs.318.14. URL <https://doi.org/10.4204/eptcs.318.14>.
- J. R. Koenig, O. Padon, and A. Aiken. Adaptive restarts for stochastic synthesis. In S. N. Freund and E. Yahav, editors, *PLDI '21: 42nd ACM SIGPLAN International Conference on Programming Language Design and Implementation, Virtual Event, Canada, June 20-25, 2021*, pages 696–709. ACM, 2021. doi: 10.1145/3453483.3454071. URL <https://doi.org/10.1145/3453483.3454071>.
- G. Li, Y. Ding, and Y. Xie. Tackling the qubit mapping problem for nisq-era quantum devices, 2018. URL <https://arxiv.org/abs/1809.02573>.
- V. Mnih, A. P. Badia, M. Mirza, A. Graves, T. Lillicrap, T. Harley, D. Silver, and K. Kavukcuoglu. Asynchronous methods for deep reinforcement learning. In *International conference on machine learning*, pages 1928–1937. PMLR, 2016.
- T. Monz, D. Nigg, E. A. Martinez, M. F. Brandl, P. Schindler, R. Rines, S. X. Wang, I. L. Chuang, and R. Blatt. Realization of a scalable shor algorithm. *Science*, 351(6277):1068–1070, 2016.
- Y. Nam, N. J. Ross, Y. Su, A. M. Childs, and D. Maslov. Automated optimization of large quantum circuits with continuous parameters. *npj Quantum Information*, 4(1):1–12, 2018.
- M. Ostaszewski, L. M. Trenkwalder, W. Masarczyk, E. Scerri, and V. Dunjko. Reinforcement learning for optimization of variational quantum circuit architectures. *Advances in Neural Information Processing Systems*, 34:18182–18194, 2021.
- A. Paszke, S. Gross, F. Massa, A. Lerer, J. Bradbury, G. Chanan, T. Killeen, Z. Lin, N. Gimelshein, L. Antiga, A. Desmaison, A. Kopf, E. Yang, Z. DeVito, M. Raison, A. Tejani, S. Chilamkurthy, B. Steiner, L. Fang, J. Bai, and S. Chintala. Pytorch: An imperative style, high-performance deep learning library. In H. Wallach, H. Larochelle, A. Beygelzimer, F. d'Alché-Buc, E. Fox, and R. Garnett, editors, *Advances in Neural Information Processing Systems 32*, pages 8024–8035. Curran Associates, Inc., 2019. URL <http://papers.nips.cc/paper/9015-pytorch-an-imperative-style-high-performance-deep-learning-library.pdf>.
- A. Peruzzo, J. McClean, P. Shadbolt, M.-H. Yung, X.-Q. Zhou, P. J. Love, A. Aspuru-Guzik, and J. L. O'brien. A variational eigenvalue solver on a photonic quantum processor. *Nature communications*, 5(1):1–7, 2014a.
- A. Peruzzo, J. McClean, P. Shadbolt, M.-H. Yung, X.-Q. Zhou, P. J. Love, A. Aspuru-Guzik, and J. L. O'brien. A variational eigenvalue solver on a photonic quantum processor. *Nature communications*, 5(1):4213, 2014b.
- J. Pointing, O. Padon, Z. Jia, H. Ma, A. Hirth, J. Palsberg, and A. Aiken. Quanto: Optimizing quantum circuits with automatic generation of circuit identities. *arXiv:2111.11387*, 2021. URL <https://doi.org/10.48550/arXiv.2111.11387>.
- M. G. Pozzi, S. J. Herbert, A. Sengupta, and R. D. Mullins. Using reinforcement learning to perform qubit routing in quantum compilers. *arXiv preprint arXiv:2007.15957*, 2020.
- N. Quetschlich, L. Burgholzer, and R. Wille. MQT Bench: Benchmarking software and design automation tools for quantum computing, 2022. MQT Bench is available at <https://www.cda.cit.tum.de/mqtbench/>.
- J. Schulman, F. Wolski, P. Dhariwal, A. Radford, and O. Klimov. Proximal policy optimization algorithms. *arXiv preprint arXiv:1707.06347*, 2017.
- A. Sinha, U. Azad, and H. Singh. Qubit routing using graph neural network aided monte carlo tree search. In *Proceedings of the AAAI Conference on Artificial Intelligence*, volume 36, pages 9935–9943, 2022.

- S. Sivarajah, S. Dilkes, A. Cowtan, W. Simmons, A. Edgington, and R. Duncan. `t|ket`: a retargetable compiler for nisq devices. *Quantum Science and Technology*, 6(1):014003, Nov 2020. ISSN 2058-9565. doi: 10.1088/2058-9565/ab8e92. URL <http://dx.doi.org/10.1088/2058-9565/ab8e92>.
- M. Skilbeck, E. Peterson, appleby, E. Davis, P. Karalekas, J. M. Bello-Rivas, D. Kochmanski, Z. Beane, R. Smith, A. Shi, C. Scott, A. Paszke, E. Hulburd, M. Young, A. S. Jackson, BHAVISHYA, M. S. Alam, W. Velázquez-Rodríguez, c. b. osborn, fengdlm, and jmackeyrigetti. `rigetti/quilc`: v1.21.0, July 2020. URL <https://doi.org/10.5281/zenodo.3967926>.
- R. S. Sutton, D. McAllester, S. Singh, and Y. Mansour. Policy gradient methods for reinforcement learning with function approximation. *Advances in neural information processing systems*, 12, 1999.
- M. Wang, D. Zheng, Z. Ye, Q. Gan, M. Li, X. Song, J. Zhou, C. Ma, L. Yu, Y. Gai, et al. Deep graph library: A graph-centric, highly-performant package for graph neural networks. *arXiv preprint arXiv:1909.01315*, 2019a.
- M. Wang, D. Zheng, Z. Ye, Q. Gan, M. Li, X. Song, J. Zhou, C. Ma, L. Yu, Y. Gai, et al. Deep graph library: A graph-centric, highly-performant package for graph neural networks. *arXiv preprint arXiv:1909.01315*, 2019b.
- A. Xu, A. Molavi, L. Pick, S. Tannu, and A. Albarghouthi. Synthesizing quantum-circuit optimizers. *arXiv preprint arXiv:2211.09691*, 2022a.
- M. Xu, Z. Li, O. Padon, S. Lin, J. Pointing, A. Hirth, H. Ma, J. Palsberg, A. Aiken, U. A. Acar, and Z. Jia. Quartz: Superoptimization of quantum circuits (extended version), 2022b.
- M. Xu, Z. Li, O. Padon, S. Lin, J. Pointing, A. Hirth, H. Ma, J. Palsberg, A. Aiken, U. A. Acar, and Z. Jia. Quartz: Superoptimization of quantum circuits. In *Proceedings of the 43rd ACM SIGPLAN International Conference on Programming Language Design and Implementation (PLDI '22), June 13–17, 2022, San Diego, CA, USA*. ACM, 2022c. doi: 10.1145/3519939.3523433. URL <https://doi.org/10.1145/3519939.3523433>.

A PROOF OF THEOREM 1

PROOF. Let $NG(C, g, x)$ refer to the new gates g' introduced by x in C' . For gates $g' \in C' \wedge g' \notin IG(d, C, g, x)$, there are three cases: (1) g' is a k -hop predecessor of $NG(C, g, x)$ where $k > d$; (2) g' is a successor of $NG(C, g, x)$; (3) g' is neither a predecessor nor a successor of $NG(C, g, x)$. The availability of any transformation (G, G') where the depth of G is less than or equal to d on gate g , only depends on the d -hop successors of g . For case (1), (2) and (3), the d -hop successors of g' remains unchanged. For case (1), since g' is a k -hop predecessor of $NG(C, g, x)$ where $k > d$, then all gates in $NG(C, g, x)$ are outside g' 's d -hop successors, so g' 's d -hop successors remain unchanged. For case (2), all successors of g' are successors of $NG(C, g, x)$, remaining unchanged. For case (3), since g' is not a predecessor of $NG(C, g, x)$, none of its successors are in $NG(C, g, x)$. Thus, g' 's successors remain unchanged. \square

B DEPTH RESULTS ON THE NAM GATE SET

Table 5. Comparing Quarl and existing circuit optimizers on reducing the depth of the benchmark circuits under the Nam gate set. The best result for each circuit is in bold.

Circuit	Depth (Nam gate set)									
	Orig.	Nam	VOQC	Qiskit	Tket	Quartz w/ R.M.	Quartz w/o R.M.	Quarl w/ R.M.	Quarl w/o R.M.	
tof_3	33	31	31	33	31	31	32	29	25	
barenco_tof_3	45	38	39	45	42	37	39	32	34	
mod5_4	52	46	46	52	51	29	31	18	18	
tof_4	54	46	46	54	50	46	45	39	40	
barenco_tof_4	87	68	70	87	80	64	73	56	56	
tof_5	75	61	61	75	69	61	60	48	47	
mod_mult_55	55	47	50	54	51	45	53	41	48	
vbe_adder_3	90	58	60	96	81	60	67	43	42	
barenco_tof_5	129	95	98	129	118	90	114	79	87	
cs1a_mux_3	72	63	68	84	64	62	63	64	61	
rc_adder_6	111	83	95	111	97	90	95	74	88	
gf2^4_mult	112	102	102	110	108	105	103	87	81	
tof_10	180	136	136	180	164	136	131	122	121	
mod_red_21	176	129	135	173	150	146	176	131	135	
hwb6	178	-	153	177	157	147	173	132	130	
gf2^5_mult	146	132	131	142	141	135	150	114	133	
csum_mux_9	64	47	46	64	61	55	64	53	70	
barenco_tof_10	339	230	238	339	308	228	339	215	249	
qcla_com_7	94	70	67	99	88	66	91	76	63	
ham15-low	285	-	245	283	258	250	285	221	209	
gf2^6_mult	184	166	166	180	178	165	182	153	186	
qcla_adder_10	84	63	67	89	78	65	84	78	75	
gf2^7_mult	220	198	198	215	213	197	218	232	245	
gf2^8_mult	262	236	235	255	253	235	262	295	315	
qcla_mod_7	229	184	199	231	211	195	229	191	205	
adder_8	259	193	196	264	243	199	255	242	217	
Geo. Mean Reduction	-	19.4%	17.3%	-0.7%	7.4%	19.6%	9.1%	25.7%	23.4%	

C DEPTH RESULTS ON THE IBM GATE SET

Table 6. Comparing Quarl and existing circuit optimizers on reducing the depth of the benchmark circuits under the IBM gate set. The best result for each circuit is in bold.

Circuit	Depth (IBM gate set)				
	Orig.	Qiskit	Tket	Quartz	Quarl
tof_3	37	37	37	32	32
barenco_tof_3	50	50	50	40	39
mod5_4	57	57	57	52	47
tof_4	60	60	60	47	47
tof_5	83	83	83	64	61
barenco_tof_4	96	96	96	80	67
mod_mult_55	60	58	61	55	52
vbe_adder_3	98	99	93	73	48
barenco_tof_5	142	142	142	119	94
csla_mux_3	80	83	75	84	65
rc_adder_6	124	119	125	109	92
gf2^4_mult	117	115	114	118	95
hwb6	186	183	189	188	131
mod_red_21	183	178	201	183	128
tof_10	198	198	198	149	140
gf2^5_mult	148	144	143	149	138
csum_mux_9	68	68	77	68	84
barenco_tof_10	372	372	372	376	249
ham15-low	310	298	288	300	235
qcla_com_7	98	100	97	95	78
gf2^6_mult	189	185	184	189	197
qcla_adder_10	89	92	84	89	77
gf2^7_mult	225	220	219	225	248
gf2^8_mult	267	260	259	268	312
qcla_mod_7	241	241	235	238	250
adder_8	278	274	318	275	208
vqe_8	69	20	27	24	28
qgan_8	60	31	30	45	34
qaoa_8	56	45	42	48	51
ae_8	193	143	136	175	142
qpeexact_8	199	140	132	160	149
qpeinexact_8	212	144	146	165	156
qft_8	170	115	108	131	120
qftentangled_8	184	121	153	162	129
portfoliovqe_8	151	67	61	86	100
portfolioqaoa_8	300	232	216	288	305
Geo. Mean Reduction	-	13.5%	12.9%	13.4%	22.1%